Chemical Physics 515 (2018) 299–314

Contents lists available at ScienceDirect

Chemical Physics

journal homepage: www.elsevier.com/locate/chemphys

An efficient pseudo-spectral method for the description of atomic electronic wave functions – Application to the hydrogen atom in a uniform magnetic field

Clemens Woywod[a,1], Susmita Roy[b], Kiran Sankar Maiti[c], Kenneth Ruud[d]

[a] Department Chemie, Technische Universität München, D-85747 Garching, Germany
[b] Research Unit of Buhl-Strohmaier Foundation for Cerebral Palsy and Paediatric Neuroorthopaedics, Orthopaedic Department, Klinikum rechts der Isar, Technische Universität München, D-81675 München, Germany
[c] Max Planck Institut für Quantenoptik, Hans-Kopfermann-Str. 1, D-85748 Garching, Germany
[d] Hylleraas Centre for Quantum Molecular Sciences, Department of Chemistry, The University of Tromsø – The Arctic University of Norway, N-9037 Tromsø, Norway

ARTICLE INFO

This article is dedicated to Wolfgang Domcke on the occasion of his 70th birthday.

ABSTRACT

The mapping of an electronic state on a real-space support lattice may offer advantages over a basis set ansatz in cases where there are linear dependences due to basis set overcompleteness or when strong internal or external fields are present. Such discretization methods are also of interest because they allow for the convenient numerical integration of matrix elements of local operators. We have developed a pseudo-spectral approach to the numerical solution of the time-dependent and time-independent Schrödinger equations describing electronic motion in atoms and atomic ions in terms of a spherical coordinate system. A key feature of this scheme is the construction of a *Variational Basis Representation* (VBR) for the non-local component and of a *Generalized Finite Basis Representation* (GFBR) for the local component of the electronic Hamiltonian operator. Radial Hamiltonian eigenfunctions $\chi_{nl;\beta}(r)$ of the H atom-like system and spherical harmonics form the basis set. Two special cases of this approach are explored: In one case, the functions of the field-free H atom are used as the elements of the basis set, and in the second case, each radial basis function has been obtained by variationally optimizing a shielding parameter β to yield a minimum energy for a particular eigenstate of the H atom in a uniform magnetic field.

We derive a new quadrature rule of nearly Gaussian accuracy for the computation of matrix elements of local operators between radial basis functions and perform numerical evaluation of local operator matrix elements involving spherical harmonics. With this combination of radial and angular quadrature prescriptions we ensure to a good approximation the discrete orthogonality of Hamiltonian eigenfunctions of H atom-like systems for summation over the grid points. We further show that sets of $\chi_{nl;\beta}(r)$ functions are linearly independent, whereas sets of the polar-angle-dependent components of the spherical harmonics, i.e., the associated Legendre functions, are not and provide a physical interpretation of this mathematical observation.

The pseudo-spectral approach presented here is applied to two model systems: the field-free H atom and the H atom in a uniform magnetic field. The results demonstrate the potential of this method for the description of challenging systems such as highly charged atomic ions.

1. Introduction

Grid-based methods are commonly employed for the solution of both the time-dependent Schrödinger equation (TDSE) as well as the time-independent Schrödinger equation (TISE) that describes the nuclear dynamics of a molecule [1]. This is because grid-based methods have several attractive features for the numerical calculation of wave functions or probability densities compared to conventional basis set methods: (i) Whereas spectral methods are usually the most accurate option for solving partial differential equations due to their global nature, this is no longer the case if the functions to be approximated have sharp gradients or discontinuities (Gibbs phenomenon) [2,3]. In the context of electronic structure theory, the presence of time-dependent or time-independent strong internal or external fields may induce

[1] Present address.

https://doi.org/10.1016/j.chemphys.2018.09.025
Received 15 July 2018; Accepted 20 September 2018
Available online 27 September 2018
0301-0104/

phenomena in the state solutions analogous to shock waves in fluid mechanics, thus by analogy suggesting the benefits of grid-based methods compared to spectral methods [4]. (ii) In electronic structure theory, standard basis functions (Gaussian- or Slater-type atomic orbitals, GTOs or STOs) converge asymptotically to zero (if the respective nucleus is defined as the origin). However, they are non-local and non-orthogonal, which means that global linear dependences of the basis functions may arise [5,6]. This linear-dependence problem, which occurs for large basis sets containing diffuse functions, is due to over-completeness of the basis [7,8] and may lead to numerical instabilities. Real-space lattice methods in contrast use localized and orthogonal basis functions, thus avoiding global linear dependences [5]. Furthermore, grid points used for describing potential energy (PE) surfaces for a reaction involving two or more partners can be distributed over the complete computational cell. This makes it possible to avoid Basis-Set Superposition Errors (BSSEs) which otherwise occur in calculations employing incomplete, atom-centered basis functions [9–12]. (iii) The last aspect is of a technical nature and is to a large part responsible for the interest in grid-based methods for quantum nuclear dynamics but is also of relevance to electronic structure calculations: the avoidance of deriving exact integral solutions for the evaluation of matrix elements of local operators and the option to relinquish the construction of analytical expressions for local operators.

We discuss these differences between grid-based and spectral methods in more detail in the Appendix, where we in particular highlight situations in which these differences favor grid-based methods and where they will outperform methods based on traditional basis sets.

Of all problems in electronic structure theory, only the energy spectrum of the H atom and of the H_2^+ ion, the energy levels of a harmonic oscillator giving the spectrum of a free electron in a uniform magnetic field (Landau levels), and the H atom in an external electric field had until 1996 been solved exactly. The H atom in a uniform magnetic field thus remained as one of the prominent unsolved problems in "elementary" non-relativistic quantum mechanics [13], and has for this reason attracted significant attention [14–20]. Relativistic effects on this model system have also been considered [21].

Kravchenko et al. published in 1996 an exact solution to the Schrödinger equation of a hydrogen atom in a uniform magnetic field [13,22,23]. The solution was expressed in the form of a power series in the radial variable, and with expansion coefficients being polynomials of the sine of the polar angle. However, this solution is computationally challenging in the case of strong magnetic fields and large atomic radii, such as those relevant to excited states, due to the oscillating behaviour of the power series. Rutkowski and Poszwa later proposed an asymptotic solution in terms of a modified power series that allowed for a more efficient computation of excited states in intense magnetic fields [24]. Although an exact solution to the 'H atom in a uniform magnetic field' problem has now been provided, methods for an approximate description of the wave functions are still of interest, both because they may lead to an improved understanding of this system and because this could provide a computationally efficient route to more complex systems.

A first step in this direction was taken already in 1984 by Gallas, who, based on a study of Rydberg atoms in magnetic fields [25], introduced an elegant spectral approach using a minimal basis set [26]. Employing spherical coordinates r, θ and ϕ, the minimal basis set is constructed from modified eigenfunctions $\sigma_{nlm;\beta}(r, \theta, \phi)$ of the Hamiltonian of the field-free H atom, i.e., the basis functions are derived by replacing the atomic number 1 by a variational parameter β in the TISE for the H atom-like system. β is thus defined by minimizing the energy $E_{nlm}(\beta)$ of the H atom in a uniform magnetic field. The value of β depends on the magnetic field strength (parameter γ) as well as on the quantum numbers n, l and m of each individual state.

The average values of observables presented in Ref. [26] have been obtained by exclusively varying β. The procedure uses the fact that the eigenstates $\sigma_{nlm;\beta}(r, \theta, \phi)$ of the H atom-like system with a β-parameterized PE term are approximate solutions to the TISE for the H atom in a uniform magnetic field that can be directly utilized for the calculation of expectation values of operators. This means that a particular wave function is not expanded in terms of a comprehensive $\{\sigma_{nlm;\beta}(r, \theta, \phi)\}$ basis set, rather the ansatz defines only one basis function per state.

The key idea behind a spectral variational calculation in electronic structure theory is commonly that a physically meaningful wave function for a particular system can be obtained by linear combination of rather unspecific, general basis functions. Ref. [26] pursues an alternative route: instead of varying the coefficients of an expansion in terms of an off-the-shelf basis set, a single basis function is variationally adapted to a selected state, i.e., the expectation values are determined as elements of one-dimensional Hamiltonian 'matrices'. Even though the optimized basis functions are only approximations to the true eigenfunctions, the $E_{nlm}(\beta)$ values can be considered as upper bounds for the energy levels of the system. Ref. [26] shows that the results obtained with this computationally efficient method are quite accurate.

In the present study we also employ the $\{\sigma_{nlm;\beta}(r, \theta, \phi)\}$ basis set for the spectral representation of the 'H atom in a uniform magnetic field' Hamiltonian operator $\widehat{H}_\gamma(r, \theta, \phi)$ (*vide infra*). However, we construct a full matrix representation for the variational solution of the TISE. In addition, we implement a hybrid concept which relies on the expansion of the wave function in terms of $\sigma_{nlm;\beta}(r, \theta, \phi)$ functions for building a matrix representation of the non-local component of $\widehat{H}_\gamma(r, \theta, \phi)$, whereas a *Generalized Finite Basis Representation* (GFBR) [27] is constructed for the local component. Even though the parameter β is used for deriving the basis functions, this pseudo-spectral approach to solving the TISE, which involves the definition of a new radial quadrature rule, is non-variational and our goal is to demonstrate its accuracy.

The remainder of this article is organized as follows: In Section 2 the Hamiltonian $\widehat{H}_\gamma(r, \theta, \phi)$ is defined, Section 3 outlines fundamental aspects of matrix representations of operators like *Discrete Variable Representation* (DVR) [28,1,29,30] and GFBR. Section 4 describes the evaluation of the corresponding matrix elements. Computational results for the field-free H atom and the H atom in a uniform magnetic field are discussed in Sections 5.1 and 5.2, respectively. Finally, some concluding remarks and perspectives are given in Section 6.

2. Definition of the model Hamiltonian

Neglecting spin as well as relativistic effects and considering only the z component of the magnetic field $\vec{B}$ in the Coulomb gauge $\vec{A}(\vec{r}) = \frac{1}{2}\vec{B} \times \vec{r}$, we obtain the following Hamiltonian for a H atom in a uniform magnetic field [19]:

$$\widehat{H}_\gamma(r, \theta, \phi) := \widehat{\mathscr{H}}_{\beta=1}(r, \theta, \phi) + \frac{\gamma}{2}\hat{L}_z(\phi) + \frac{\gamma^2}{8\mu}r^2(\sin(\theta))^2, \tag{2.1}$$

$$\widehat{\mathscr{H}}_\beta(r, \theta, \phi) := -\frac{\hbar^2}{2\mu}\hat{\nabla}^2 + \beta\widehat{V}_H(r), \tag{2.2}$$

where

$$\mu := \frac{m_N m_e}{m_N + m_e}, \tag{2.3}$$

$$\widehat{V}_H(r) := -\frac{e^2}{4\pi\varepsilon_0 r}. \tag{2.4}$$

$\hbar$ is Planck's constant divided by 2π, e the electron charge, ε_0 the electric permittivity, γ ($:= B/B_0$) the magnetic field strength in atomic units of $B_0 := 2.35 \times 10^{15}$ T, while m_N and m_e are the masses of the atomic nucleus and of the electron, respectively. The symbol for the reduced mass of electron and nucleus is μ. Note that Refs. [13,26] use the approximation $\mu \approx m_e$ in the definition of $\widehat{H}_\gamma(r, \theta, \phi)$. The operators $\hat{L}_z(\phi)$ and $\widehat{\mathscr{H}}_\beta(r, \theta, \phi)$ can be identified with the z component of the azimuthal angular momentum and with the Hamiltonian of the (field-

free) H atom-like system, respectively. In Def. 2.1, the contributions $\frac{\gamma}{2}\hat{L}_z(\phi)$ and $\frac{\gamma^2}{8\mu}r^2(\sin(\theta))^2$ correspond to the conventional electronic Zeeman term [19,31] and to $|\vec{A}(\vec{r})|^2$, respectively. $\hat{V}_H(r)$ is the PE term of the field-free H atom Hamiltonian, i.e., of the operator $\hat{\mathscr{H}}_\beta(r,\theta,\phi)$ with $m_N = m_{proton}$ and $\beta = 1$.

It may appear inconsistent to use the definition of $\hat{\mathscr{H}}_{\beta=1}(r,\theta,\phi)$ in Def. 2.1 since $\gamma \neq 0$ implies $\beta \neq 1$. However, the operator $\hat{\mathscr{H}}_\beta(r,\theta,\phi)$ (Def. 2.2) in combination with $\beta \neq 1$ is exclusively used for the computation of the $\{\sigma_{nlm;\beta}(r,\theta,\phi)\}$ basis set. The parameter β does not play any role in the description of the physical system itself, as the magnetic field strength is exclusively quantified by γ in the definition of $\hat{H}_\gamma(r,\theta,\phi)$.

If we relinquish the symbols $\hat{\mathscr{H}}_{\beta=1}(r,\theta,\phi)$, $\hat{L}_z(\phi)$ and $\hat{\nabla}$, the Hamiltonian in Def. 2.1 reads in full form [13]:

$$\hat{H}_\gamma(r,\theta,\phi) = -\frac{\hbar^2}{2\mu}\left[\frac{2}{r}\frac{\partial}{\partial r} + \frac{\partial^2}{(\partial r)^2} + \frac{1}{r^2\tan(\theta)}\frac{\partial}{\partial\theta} + \frac{1}{r^2}\frac{\partial^2}{(\partial\theta)^2} + \frac{1}{r^2(\sin(\theta))^2}\frac{\partial^2}{(\partial\phi)^2}\right] + \hat{V}_H(r) - \frac{i\gamma\hbar}{2}\frac{\partial}{\partial\phi} + \frac{\gamma^2}{8\mu}r^2(\sin(\theta))^2. \tag{2.5}$$

We partition the Hamiltonian according to local ($\hat{H}_{loc}$) and non-local, or global, ($\hat{H}_{glo}$) components:

$$\hat{H}_\gamma(r,\theta,\phi) = \underbrace{\hat{T}_H(r,\theta,\phi) - \frac{\gamma}{2}i\hbar\frac{\partial}{\partial\phi}}_{\hat{H}_{glo}} + \underbrace{\hat{V}_H(r) + \frac{\gamma^2}{8\mu}r^2(\sin(\theta))^2}_{\hat{H}_{loc}}, \tag{2.6}$$

$$\hat{T}_H(r,\theta,\phi) := \frac{1}{2\mu r^2}\left[-\hbar^2\frac{\partial}{\partial r}\left(r^2\frac{\partial}{\partial r}\right) + \hat{L}^2(\theta,\phi)\right], \tag{2.7}$$

$$\hat{L}^2(\theta,\phi) := -\hbar^2\left(\frac{\partial^2}{(\partial\theta)^2} + \cot(\theta)\frac{\partial}{\partial\theta} + \frac{1}{(\sin(\theta))^2}\frac{\partial^2}{(\partial\phi)^2}\right), \tag{2.8}$$

where $\hat{T}_H(r,\theta,\phi)$ (with $m_N = m_{proton}$) is the kinetic energy term of $\hat{\mathscr{H}}_\beta(r,\theta,\phi)$, and $\hat{L}^2(\theta,\phi)$ represents the square of the orbital angular momentum operator.

The separation of $\hat{H}_\gamma(r,\theta,\phi)$ into $\hat{H}_{glo}$ and $\hat{H}_{loc}$ is important for the pseudo-spectral approach described in this study: Operators such as $\hat{H}_{loc}$ that are local in coordinate space can be represented on a real-space grid, i.e., in terms of infinitely localized basis functions, whereas a basis set of globally defined and differentiable functions is required for the representation of non-local operators such as $\hat{H}_{glo}$.

3. Construction of the Hamiltonian matrix: VBR, DVR, FBR and GFBR

3.1. Definition of VBR

It is useful for the following discussion to differentiate between operator representations based on whether the matrix elements can be evaluated exactly or only approximately. A *Variational Basis Representation* (VBR) [28,1,30] denotes an exact matrix representation of an operator $\hat{O}(x)$ in terms of a set of ${}^{\mathrm{VBR}}N$ basis functions ($\{\kappa_m(x)\}$), where the matrix elements are defined as $O_{mn} := \langle\kappa_m(x)|\hat{O}(x)|\kappa_n(x)\rangle$. The name VBR derives from the fact that the eigenvalues $\omega_k^{({}^{\mathrm{VBR}}N)}$ of a ${}^{\mathrm{VBR}}N$ function representation of $\hat{O}(x)$ fulfill the condition $\omega_k^{({}^{\mathrm{VBR}}N)} \geqslant \omega_k$, ω_k being the true eigenvalues of $\hat{O}(x)$.

In the present study the variational principle is actually applied twice in the calculation of eigenvalues of the VBR matrix of $\hat{H}_\gamma(r,\theta,\phi)$ constructed from the set $\{\sigma_{nlm;\beta}(r,\theta,\phi)\}$: (i) each basis function is optimized to approximate an eigenstate of $\hat{H}_\gamma(r,\theta,\phi)$ by varying the parameter β as described in Ref. [26], and (ii) each eigenfunction of the VBR matrix of $\hat{H}_\gamma(r,\theta,\phi)$ is a linear expansion in terms of the set $\{\sigma_{nlm;\beta}(r,\theta,\phi)\}$ with variationally determined expansion coefficients.

3.2. Definition of DVR

The already mentioned DVR corresponds to a representation in terms of ${}^{\mathrm{VBR}}N$ basis functions which are infinitely localized at the grid points [30]. In the DVR, the diagonal elements of a local operator matrix are obtained by evaluation of the operator at the ${}^{\mathrm{VBR}}N$ grid points, the off-diagonal elements being zero.

3.3. Definitions of FBR and GFBR as well as relations to the DVR

The GFBR and its special variant, the *Finite Basis Representation* (FBR), of $\hat{O}(x)$ are approximations to the VBR in the sense that the matrix elements are not evaluated exactly but are rather computed numerically by employing a common quadrature rule for all integrals. Compared to the VBR, this allows for a straightforward representation of local operators: to construct a FBR or GFBR of such an operator, it suffices to determine the values of a local operator at the grid points. In contrast, to obtain a VBR of a local operator, the dependence of the operator on the spatial coordinates must be known globally. In general, due to the numerical quadrature, the eigenvalues $\tilde{\omega}_k^{({}^{\mathrm{VBR}}N)}$ of the ${}^{\mathrm{VBR}}N$-dimensional FBR or GFBR matrix of operator $\hat{O}(x)$ are not variational unless an exact quadrature result is used for all matrix elements.

The DVR and FBR matrices are unitarily equivalent [32,33,28,1,30,27] and the quadrature rule employed for the calculation of the FBR approximation to the elements of the VBR matrix of a local operator defines the unitary transformation of the, in general, non-diagonal FBR matrix into the diagonal DVR matrix. The equivalence between the DVR and FBR implies that the number of VBR basis functions ${}^{\mathrm{VBR}}N$ must be identical to the number of DVR grid points.

In the GFBR framework, we only request that one common quadrature rule based on ${}^{\mathrm{GFBR}}N$ grid points is applied to the evaluation of the GFBR matrix elements of a local operator, but we generally do not impose any restriction on ${}^{\mathrm{GFBR}}N$, and ${}^{\mathrm{GFBR}}N$ may therefore differ from ${}^{\mathrm{VBR}}N$ [27]. The use of this common quadrature rule for the construction of a diagonal DVR matrix representation of a local operator via a unitary transformation is, however, only possible if ${}^{\mathrm{GFBR}}N = {}^{\mathrm{VBR}}N$.

The implementation of a quadrature rule in which ${}^{\mathrm{GFBR}}N \neq {}^{\mathrm{VBR}}N$ will eliminate the option to unitarily transform the Hamiltonian matrix from the GFBR into the DVR. Nevertheless, this is not expected to significantly impair the computational performance when solving the TISE, as the Hamiltonian matrix is in general non-diagonal also in the DVR due to the contribution of matrix representations of non-local operators. The main advantage of pseudo-spectral methods, i.e. the construction of matrix representations of local operators via direct evaluation at the grid points, can therefore also be realized and applied even if ${}^{\mathrm{GFBR}}N \neq {}^{\mathrm{VBR}}N$.

3.4. Definitions of VBR and GFBR Hamiltonian matrices

For the solution of the TISE for the 'H atom in a uniform magnetic field' system, we will focus on two Hamiltonian matrix constructions:

$$\mathbf{H}_1 := {}^{\mathrm{VBR}}\mathbf{H}_{glo} + {}^{\mathrm{VBR}}\mathbf{H}_{loc}, \tag{3.1}$$

$$\mathbf{H}_2 := {}^{\mathrm{VBR}}\mathbf{H}_{glo} + {}^{\mathrm{GFBR}}\mathbf{H}_{loc}. \tag{3.2}$$

$\mathbf{H}_1$ here corresponds to the VBR or spectral representation of $\hat{H}_\gamma(r,\theta,\phi)$, $\mathbf{H}_2$ to a pseudo-spectral representation, the GFBR.

We note that in the case of $\mathbf{H}_2$, even though it is described as a GFBR representation, it is composed of both a VBR and a GFBR component, since it is not possible to represent non-local operators in terms of infinitely localized basis functions as required for the construction of a DVR, FBR or of a GFBR [30].

The eigenvalues of $\mathbf{H}_1$ and $\mathbf{H}_2$ are always variational and normally non-variational, respectively. Again, eigenvalues of $\mathbf{H}_2$ can become variational if the quadrature approximation of all elements of ${}^{\mathrm{GFBR}}\mathbf{H}_{loc}$

yields exact solutions.

Interestingly, the case ${}^{\mathrm{GFBR}}\mathbf{H}_{loc} \neq {}^{\mathrm{VBR}}\mathbf{H}_{loc}$ provides two related, but conceptually different reasons for the non-variational nature of the eigenvalues $\widetilde{\omega}_k^{({}^{\mathrm{VBR}}N)}$ of $\mathbf{H}_2$: in addition to the numerical quadrature error, which is responsible for non-variational eigenvalues of the component ${}^{\mathrm{GFBR}}\mathbf{H}_{loc}$, it also reflects the inconsistency in the basis set representation of the operators $\widehat{H}_{glo}$ and $\widehat{H}_{loc}$.

In practice, the scenario ${}^{\mathrm{GFBR}}N > {}^{\mathrm{VBR}}N$ is very common since a dense quadrature lattice may be needed to reach a convergence of the approximation ${}^{\mathrm{GFBR}}\mathbf{H}_{loc}$ to ${}^{\mathrm{VBR}}\mathbf{H}_{loc}$. The value of ${}^{\mathrm{VBR}}N$ required to obtain converged eigenvalues of $\mathbf{H}_1$ is typically much smaller than the critical limit of ${}^{\mathrm{GFBR}}N$. The dimension of $\mathbf{H}_1$ required for the accurate computation of the energy spectrum of interest also applies to $\mathbf{H}_2$. This means that it is usually not a reasonable option to increase ${}^{\mathrm{VBR}}N$ until the condition ${}^{\mathrm{GFBR}}N = {}^{\mathrm{VBR}}N$ is met in order to be able to unitarily transform $\mathbf{H}_2$ into the DVR. As mentioned above, there is also no significant advantage in solving the TISE in the DVR as compared to directly diagonalizing $\mathbf{H}_2$.

4. Evaluation of matrix elements

4.1. Definition of basis functions

We assume that the basis functions $\sigma_{nlm;\beta}(r,\theta,\phi) \coloneqq \chi_{nl;\beta}(r)Y_l^m(\theta,\phi)$ are the usual normalized eigensolutions of the Hamiltonian $\widehat{\mathscr{H}}_\beta(r,\theta,\phi)$ (Def. 2.2) with a variationally determined parameter β and $m_N = m_{proton}$ [26].

As compared to the eigenstates of the field-free H atom, the set $\{\sigma_{nlm;\beta}(r,\theta,\phi)\}$ differs only with respect to the radial components $\chi_{nl;\beta}(r)$ if $\beta \neq 1$:

$$\chi_{nl;\beta}(r) \coloneqq \sqrt{\left(\frac{2\beta}{na_\mu}\right)^3 \frac{(n-l-1)!}{2n[(n+l)!]}}\exp\left(-\frac{\beta r}{na_\mu}\right)\left(\frac{2\beta r}{na_\mu}\right)^l L_{n-l-1}^{2l+1}\left(\frac{2\beta r}{na_\mu}\right), \tag{4.1}$$

where

$$a_\mu \coloneqq \frac{4\pi\varepsilon_0\hbar^2}{\mu e^2}, \tag{4.2}$$

and $L_{n-l-1}^{2l+1}(x)$ are generalized Laguerre polynomials.

Orthonormal eigenfunctions of $\hat{L}^2(\theta,\phi)$ are the spherical harmonics:

$$Y_l^m(\theta,\phi) \coloneqq \zeta_{lm}(\theta)\nu_m(\phi), \tag{4.3}$$

here defined as a product of the normalized functions:

$$\nu_m(\phi) \coloneqq \frac{1}{\sqrt{2\pi}}\exp(im\phi), \tag{4.4}$$

$$\zeta_{lm}(\theta) \coloneqq \sqrt{2\pi}\sqrt{\frac{(2l+1)(l-m)!}{4\pi(l+m)!}}(-1)^m P_l^m(\cos(\theta)). \tag{4.5}$$

Note that the components $P_l^m(\cos(\theta))$ do not include the Condon-Shortley phase factor $(-1)^m$. The symbol $P_l^m(x)$ represents generally an associated Legendre function of the first kind.

Because we employ a VBR product basis set defined in terms of eigenfunctions of a H atom-like system, the dimensions of the radial and of the two angular basis set components are determined by the maximum value of n (n_{max}). The size N_r of the radial basis set $\{\chi_{nl;\beta}(r)\}$ depends on n_{max} because of the coupling to the angular degrees of freedom. The possible values for the index l imply that the values $n_{max} = 1, 2, 3, \ldots$ lead to $N_r = 1, 3, 6, \ldots$ etc. N_r can also be identified with the number of radial grid points n_k in the GFBR (cf. Section 4.4.1).

The angular VBR basis dimensions ${}^{\mathrm{VBR}}N_\theta$ and ${}^{\mathrm{VBR}}N_\phi$ for $n_{max} = 1, 2, 3, \ldots$ are in an analogous manner given by ${}^{\mathrm{VBR}}N_\theta = 1, 4, 9, \ldots$ and ${}^{\mathrm{VBR}}N_\phi = 1, 3, 5, \ldots$, respectively. As will be outlined in Section 4.4.3, the GFBR grid sizes ${}^{\mathrm{GFBR}}N_\phi$ and ${}^{\mathrm{GFBR}}N_\theta$ are independent of the scale of the angular VBR basis sets.

4.2. Representation of $\widehat{H}_{glo}$ in the VBR

We first define a symbol for the overlap matrix element between two functions $\chi_{nl;\beta}(r)$ and $\chi_{n'l';\beta'}(r)$:

$$I^{\chi}_{n,l,n',l';\beta,\beta'} \coloneqq \int_0^\infty r^2\mathrm{d}r\,\chi_{nl;\beta}(r)\chi_{n'l';\beta'}(r). \tag{4.6}$$

Note that the elements of the set $\{\chi_{nl;\beta}(r)\}$ are in general not orthonormal. We will discuss this at more length in Section 4.4.1.

A VBR matrix element of $\widehat{H}_{glo}$ can be written as:

$$\begin{aligned}&\int_0^\infty r^2\mathrm{d}r\int_0^\pi \sin(\theta)\,\mathrm{d}\theta\int_0^{2\pi}\mathrm{d}\phi\\ &\times\chi_{nl;\beta}(r)\zeta_{lm}(\theta)\nu_m(\phi)\Bigg[\Bigg(\widehat{T}_H(r,\theta,\phi)\\ &-\frac{\gamma}{2}i\hbar\frac{\partial}{\partial\phi}\Bigg)(\nu_{m'}(\phi))^*\zeta_{l'm'}(\theta)\chi_{n'l';\beta'}(r)\Bigg].\end{aligned} \tag{4.7}$$

Substituting $\widehat{T}_H(r,\theta,\phi)$ using Def. 2.7, we obtain:

$$\begin{aligned}&\int_0^\infty r^2\mathrm{d}r\,\chi_{nl;\beta}(r)\left[\left(-\frac{\hbar^2}{2\mu r^2}\right)\frac{\partial}{\partial r}\left(r^2\frac{\partial}{\partial r}\right)\chi_{n'l';\beta'}(r)\right]\int_0^\pi\zeta_{lm}(\theta)\zeta_{l'm'}\\ &(\theta)\sin(\theta)\mathrm{d}\theta\times\int_0^{2\pi}\nu_m(\phi)(\nu_{m'}(\phi))^*\mathrm{d}\phi\\ &+\int_0^\infty r^2\mathrm{d}r\,\chi_{nl;\beta}(r)\left(-\frac{\hbar^2}{2\mu r^2}\right)\chi_{n'l';\beta'}(r)\\ &\times\int_0^\pi\sin(\theta)\mathrm{d}\theta\int_0^{2\pi}\mathrm{d}\phi\,\zeta_{lm}(\theta)\nu_m(\phi)\Bigg[\Bigg(\frac{\partial^2}{(\partial\theta)^2}+\cot(\theta)\frac{\partial}{\partial\theta}\\ &+\frac{1}{(\sin(\theta))^2}\frac{\partial^2}{(\partial\phi)^2}\Bigg)(\nu_{m'}(\phi))^*\zeta_{l'm'}(\theta)\Bigg]+I^{\chi}_{n,l,n',l';\beta,\beta'}\\ &\times\left(\int_0^\pi\sin(\theta)\mathrm{d}\theta\,\zeta_{lm}(\theta)\zeta_{l'm'}(\theta)\right)\\ &\times\left(-\frac{\gamma}{2}i\hbar\int_0^{2\pi}\mathrm{d}\phi\,\nu_m(\phi)\left[\frac{\partial}{\partial\phi}(\nu_{m'}(\phi))^*\right]\right)\coloneqq A+B+C.\end{aligned} \tag{4.8}$$

The matrix elements A, B and C have been calculated as follows:

$$A=\left(-\frac{\hbar^2}{2\mu}\right)\left(\int_0^\infty r^2\mathrm{d}r\,\chi_{nl;\beta}(r)\left[\left(\frac{1}{r^2}\right)\frac{\partial}{\partial r}\left(r^2\frac{\partial}{\partial r}\right)\chi_{n'l';\beta'}(r)\right]\right)\delta_{ll'}\delta_{mm'}. \tag{4.9}$$

Matrix element A has been computed numerically with MATLAB [34,35].

$$\begin{aligned}B=&\left(-\frac{\hbar^2}{2\mu}\right)\int_0^\infty r^2\mathrm{d}r\,\chi_{nl;\beta}(r)\left(\frac{1}{r^2}\right)\chi_{n'l';\beta'}(r)\\ &\times\int_0^\pi\sin(\theta)\mathrm{d}\theta\int_0^{2\pi}\mathrm{d}\phi\,\zeta_{lm}(\theta)\nu_m(\phi)\Bigg[\Bigg(\frac{\partial^2}{(\partial\theta)^2}+\cot(\theta)\frac{\partial}{\partial\theta}\\ &+\frac{1}{(\sin(\theta))^2}\frac{\partial^2}{(\partial\phi)^2}\Bigg)(\nu_{m'}(\phi))^*\zeta_{l'm'}(\theta)\Bigg]\coloneqq B1\times B2,\end{aligned} \tag{4.10}$$

$$B1=\left(-\frac{\hbar^2}{2\mu}\right)\int_0^\infty r^2\mathrm{d}r\,\chi_{nl;\beta}(r)\left(\frac{1}{r^2}\right)\chi_{n'l;\beta'}(r). \tag{4.11}$$

Only matrix elements $B1$ between $\chi_{nl;\beta}(r)$ and $\chi_{n'l;\beta'}(r)$ functions, i.e., between functions with common index l, can contribute to the VBR of $\widehat{H}_{glo}$ due to the factor $B2$ (*vide infra*). If $\beta = \beta' = 1$ and $n = n'$ the value of the integral is:

$$B1 = -\frac{\hbar^2}{2\mu}\frac{1}{n^3(l+0.5)}. \tag{4.12}$$

Non-zero values of $B1$ are also obtained if $\beta = \beta' = 1$ and $n \neq n'$. These off-diagonal matrix elements have been computed numerically with MATLAB [34,35]. When $\beta, \beta' \neq 1$, both the diagonal and off-diagonal matrix elements $B1$ have been calculated by numerical integration using MATLAB [34,35].

$B2$ has an analytic form, and is given by:

$$B2 = \int_0^{\pi} \sin(\theta)\mathrm{d}\theta \int_0^{2\pi} \mathrm{d}\phi\, \zeta_{lm}(\theta)\nu_m(\phi)\left[\left(\frac{\partial^2}{(\partial\theta)^2} + \cot(\theta)\frac{\partial}{\partial\theta} + \frac{1}{(\sin(\theta))^2}\frac{\partial^2}{(\partial\phi)^2}\right)(\nu_{m'}(\phi))^*\zeta_{l'm'}(\theta)\right] = (-l(l+1))\delta_{ll'}\delta_{mm'}. \tag{4.13}$$

For C, we get:

$$C = I^{\chi}_{n,l,n',l';\beta,\beta'} \times \left(\int_0^{\pi} \sin(\theta)\mathrm{d}\theta\, \zeta_{lm}(\theta)\zeta_{l'm'}(\theta)\right) \times \left(-\frac{\gamma}{2}i\hbar\int_0^{2\pi}\mathrm{d}\phi\, \nu_m(\phi)\left[\frac{\partial}{\partial\phi}(\nu_{m'}(\phi))^*\right]\right) = \frac{\gamma}{2}mI^{\chi}_{n,l,n',l;\beta,\beta'}\delta_{ll'}\delta_{mm'}. \tag{4.14}$$

If $\beta = \beta' = 1$ then:

$$C = \frac{\gamma}{2}m\delta_{nn'}\delta_{ll'}\delta_{mm'}, \tag{4.15}$$

whereas when $\beta, \beta' \neq 1$, the integral $I^{\chi}_{n,l,n',l;\beta,\beta'}$, and therefore also the matrix elements C, have been computed numerically with MATLAB [34,35].

4.3. Representation of $\widehat{H}_{loc}$ in the VBR

A VBR matrix element of $\widehat{H}_{loc}$ can be evaluated as:

$$\begin{aligned}&\int_0^{\infty} r^2\mathrm{d}r \int_0^{\pi} \sin(\theta)\mathrm{d}\theta \int_0^{2\pi} \mathrm{d}\phi\, \chi_{nl;\beta}(r)\zeta_{lm}(\theta)\nu_m(\phi) \times \left(\widehat{V}_H(r) + \frac{\gamma^2}{8\mu}r^2(\sin(\theta))^2\right)(\nu_{m'}(\phi))^*\zeta_{l'm'}(\theta)\chi_{n'l';\beta'}(r)\\ &= \left(-\frac{e^2}{4\pi\varepsilon_0}\right)\underbrace{\left(\int_0^{\infty} r^2\mathrm{d}r\, \chi_{nl;\beta}(r)\left(\frac{1}{r}\right)\chi_{n'l;\beta'}(r)\right)}_{\text{Integral } D \text{ (Eq. (8) of Ref. [26] for } n=n')}\delta_{ll'}\delta_{mm'}\\ &\quad + \frac{\gamma^2}{8\mu}\underbrace{\left(\int_0^{\infty} r^2\mathrm{d}r\, \chi_{nl;\beta}(r)r^2\chi_{n'l';\beta'}(r)\right)}_{\text{Integral } E \text{ (Eq. (7) of Ref. [26] for } n=n',l=l')}\\ &\quad \times \underbrace{\left(\int_0^{\pi} \sin(\theta)\mathrm{d}\theta\, \zeta_{lm}(\theta)(\sin(\theta))^2\zeta_{l'm}(\theta)\right)}_{\text{Integral } F \text{ (Eq. (6) of Ref. [26] for } l=l')}\delta_{mm'}.\end{aligned} \tag{4.16}$$

This leads to the following expression for the diagonal matrix elements:

$$\delta_{nn'}\delta_{ll'}\delta_{mm'}\left[\left(\frac{e^2}{4\pi\varepsilon_0}\right)\frac{\beta}{n^2} + \frac{\gamma^2}{8\mu}\frac{1}{2}\frac{n^2}{\beta^2}(5n^2 - 3l(l+1)+1) \times 2\frac{l(l+1)+m^2-1}{(2l+3)(2l-1)}\right]. \tag{4.17}$$

The integral D is non-zero if $n \neq n'$, integral E is non-zero for combinations of indices $(n \neq n', l \neq l')$, $(n = n', l \neq l')$, $(n \neq n', l = l')$ and integral F is non-zero if $l \neq l'$. Off-diagonal VBR matrix elements of $\widehat{H}_{loc}$ with combinations of indices $(n \neq n', l \neq l')$, $(n = n', l \neq l')$ and $(n \neq n', l = l')$ have been computed numerically with MATLAB [34,35].

4.4. Construction of GFBR matrices of local operators

4.4.1. H atom-like system: non-orthogonality of r- and θ-dependent wave function factors

In order to derive a quadrature rule appropriate for the evaluation of matrix elements of ${}^{\mathrm{GFBR}}\mathbf{H}_{loc}$, we start by observing that the r-, θ- and ϕ-dependent factors of $\sigma_{nlm;\beta}(r,\theta,\phi)$, i.e., the $\chi_{nl;\beta}(r)$, $\zeta_{lm}(\theta)$ and $\nu_m(\phi)$ functions, have different orthogonality properties. For the admissible values of n, l and m, the only fully orthonormal set is $\{\nu_m(\phi)\}$. In contrast, the orthonormality condition only holds for subsets of the sets $\{\chi_{nl;\beta=1}(r)\}$ and $\{\zeta_{lm}(\theta)\}$. To see this, we take a closer look at the properties of the sets $\{\chi_{nl;\beta}(r)\}$ and $\{\zeta_{lm}(\theta)\}$.

The set $\{\chi_{nl;\beta}(r)\}$ is composed of normalized eigenfunctions of the radial TISE for the H atom-like system with $m_N = m_{proton}$ and effective nuclear charge β:

$$\left[\frac{\hbar^2}{2\mu}\left(-\frac{\partial^2}{(\partial r)^2} - \frac{2}{r}\frac{\partial}{\partial r} + l(l+1)\frac{1}{r^2}\right) + \beta\widehat{V}_H(r)\right]\chi_{nl;\beta}(r) = E_n\chi_{nl;\beta}(r), \tag{4.18}$$

where

$$E_n = -\frac{\mu e^4\beta^2}{2\hbar^2 n^2}. \tag{4.19}$$

Let us first consider the field-free H atom case ($\beta = 1$). Due to the dependence of the radial Hamiltonian on l (for $n > 1$), the set $\{\chi_{nl;\beta=1}(r)\}$ includes eigenfunctions of two, three or more (depending on n) different operators. Only radial basis functions with a common index l are therefore orthonormal:

$$\int_0^{\infty} r^2\mathrm{d}r\, \chi_{nl;\beta=1}(r)\chi_{n'l;\beta=1}(r) = \delta_{nn'}, \tag{4.20}$$

while any other combination of indices n, n', l and l' yields non-zero overlap matrix elements. Note that the orthogonality property Eq. (4.20) is lost if $\gamma \neq 0$ because β then no longer is equal to 1. The overlap matrix of the set $\{\chi_{nl;\beta}(r)\}$ is in this case a full matrix and the set $\{\sigma_{nlm;\beta}(r,\theta,\phi)\}$ is no longer orthonormal.

The loss of orthonormality of the set $\{\sigma_{nlm;\beta}(r,\theta,\phi)\}$ for $\beta \neq 1$ means that the accuracy of the quadrature rule for the evaluation of GFBR matrix elements of local operators between $\sigma_{nlm;\beta}(r,\theta,\phi)$ basis functions derived in Sections 4.4.2 (radial) and 4.4.3 (angular) is reduced. The validity of the condition $\beta = 1$ is not required for orthonormalization of the set $\{\chi_{nl;\beta}(r)\}$ and a high quality radial quadrature rule can therefore still be formulated if $\beta \neq 1$ (cf. Section 4.4.2). However, a quadrature rule of Gaussian accuracy for matrix elements generally implies two properties of the basis set: (i) orthonormality in the VBR and (ii) discrete orthonormality in the GFBR. These terms can obviously not be satisfied if $\beta \neq 1$ since the set $\{\sigma_{nlm;\beta}(r,\theta,\phi)\}$ is not orthonormal in the VBR in this case.

The overlap matrices of the sets $\{\zeta_{lm}(\theta)\}$ have similar features to the overlap matrices of the sets $\{\chi_{nl;\beta=1}(r)\}$. The $\zeta_{lm}(\theta)$ functions are normalized associated Legendre functions $P_l^m(\cos(\theta))$ (Def. 4.5). $P_l^m(x)$ are solutions of the general Legendre ordinary differential equation, which can be written in Sturm–Liouville form as [36]:

$$\left[\frac{\mathrm{d}}{\mathrm{d}x}\left((1-x^2)\frac{\mathrm{d}}{\mathrm{d}x}\right) + \left(l(l+1) - \frac{m^2}{1-x^2}\right)\right]P_l^m(x) = 0. \tag{4.21}$$

Both $-l(l+1)$ and m^2 can be interpreted as eigenvalues in Eq. (4.21) and the weight functions for the set $\{P_l^m(x)\}$ on the interval [-1,1] are consequently 1 and $1/(1-x^2)$, respectively. For the H atom wave function, $-l(l+1)$ is the relevant eigenvalue in Eq. (4.21). For $l > 0$, the eigenfunctions of Eq. (4.21) with eigenvalue $-l(l+1)$ correspond to two or more operators, i.e., m^2 can take values 0, 1, 4, etc., and $\{P_l^m(x)\}$ is therefore, as is the set $\{\chi_{nl;\beta=1}(r)\}$, an inhomogeneous set of

eigenfunctions of multiple operators.

The appropriate weight function for the set $\{\zeta_{lm}(\theta)\}$ on the interval $[0,\pi]$ is $\sin(\theta)$, corresponding to a weight function 1 for the set $\{P_l^m(x)\}$ on the interval $[-1,1]$, and Eq. (4.21) shows that (for $0 \leqslant m \leqslant l$) only subsets with a common value of m are orthonormal:

$$\int_0^\pi \sin(\theta)\mathrm{d}\theta\, \zeta_{lm}(\theta)\zeta_{l'm}(\theta) = \delta_{ll'}. \tag{4.22}$$

Because the range of m for the spherical harmonics $Y_l^m(\theta, \phi)$ is defined as $-l \leqslant m \leqslant l$, we also need to address off-diagonal overlap matrix elements between functions $P_l^m(x)$ and $P_l^{\bar{m}}(x)$ with $\bar{m} = -m$:

$$\int_{-1}^{1} \mathrm{d}x\, P_l^m(x)\, P_l^{\bar{m}}(x) \neq 0. \tag{4.23}$$

The functions $P_l^m(x)$ and $P_l^{\bar{m}}(x)$ are eigenfunctions of a common operator (since $m^2 = \bar{m}^2$) and such an off-diagonal entry may therefore be expected to vanish due to orthogonality. This, however, is not the case, because:

$$P_l^{\bar{m}} = (-1)^m \frac{(l-m)!}{(l+m)!} P_l^m(x). \tag{4.24}$$

Non-zero overlap matrix elements of the set $\{\zeta_{lm}(\theta)\}$ are accordingly obtained for all combinations of indices l, l', m and m' if $m \neq m'$.

The orthonormality of the set $\{\sigma_{nlm;\beta=1}(r, \theta, \phi)\}$ is ensured through the coupling of the two components to sets of functions which are fully orthonormal: the off-diagonal non-zero elements of the overlap matrices of the sets $\{\chi_{nl;\beta=1}(r)\}$ and $\{\zeta_{lm}(\theta)\}$ are eliminated through multiplication of r- and θ-dependent factors with basis functions included in the sets $\{Y_l^m(\theta, \phi)\}$ and $\{\nu_m(\phi)\}$, respectively.

The sets $\{\chi_{nl;\beta=1}(r)\}$ and $\{\zeta_{lm}(\theta)\}$ have similar structures of the overlap matrices, but we also note an important distinctive feature: whereas the functions included in the set $\{\zeta_{lm}(\theta)\}$ are not linearly independent [37], this is not the case for the set $\{\chi_{nl;\beta=1}(r)\}$.

Because the basis functions $\sigma_{nlm;\beta=1}(r, \theta, \phi)$ are eigenfunctions of the H atom Hamiltonian, the fact that the r- and θ-dependent components can and cannot be orthonormalized, respectively, bears a physical significance for the electronic motion. A homogeneous set of eigenstates, i.e., a set of eigenfunctions of a common operator, which may include non-orthogonal degenerate eigenfunctions, can generally be orthogonalized. The absence of non-zero off-diagonal entries from the overlap matrix of a homogeneous set of eigenstates implies that the particle orbits in each state are decoupled.

A prominent example for the use of a homogeneous set of eigenfunctions as an orthonormal basis set is the representation of quantum-dynamical operators in terms of harmonic oscillator eigenstates. Like the harmonic oscillator basis set, also the set $\{\nu_m(\phi)\}$ is formed by adapting a homogeneous set of solutions to the TISE, in this case for the free-particle Hamiltonian. Both basis sets are orthonormal, however, the reasons for this common property are interestingly different: (i) The solutions to the TISE for the harmonic oscillator can be normalized to obtain the basis functions. (ii) The globally defined solutions to the free-particle TISE are, unlike bound states, not normalizable and not yielding eigenvalues that would form a discrete energy spectrum. The orthonormality of the set $\{\nu_m(\phi)\}$ is instead accomplished by imposing the definition interval $[0, 2\pi]$.

If we ignore for a moment that the $\chi_{nl;\beta=1}(r)$ and $\zeta_{lm}(\theta)$ functions are factors of eigenstates of three- ($\hat{\mathscr{H}}_\beta(r, \theta, \phi)$) and two- ($\hat{L}^2(\theta, \phi)$) dimensional operators, respectively, and consider them as abstracted orbitals describing one-dimensional electronic motion, then the observation that the elements of set $\{\chi_{nl;\beta=1}(r)\}$ are linearly independent and permit the construction of an orthormalized set $\{\widetilde{\chi}_{nl;\beta=1}(r)\}$, while the functions included in the set $\{\zeta_{lm}(\theta)\}$ are not, is of relevance for the understanding of the role of the r-, θ- and ϕ-dependent factors in the H atom wave function.

The volume of a parallelepiped spanned by three vectors is maximized if the vectors are orthogonal to each other [38]. This fact is related to Weyl's law for a region of phase space of a given volume which states that a homogeneous orthogonal set of eigenfunctions, which includes solutions to a specific TISE, e.g., describing the harmonic oscillator, pack the region at the maximum density [39]. This property can be complemented by the observation that the homogeneous set of orthogonal solutions of an eigenvalue equation represents a minimum of interstate coupling.

It thus can be inferred that linear independence of an inhomogeneous set of non-orthogonal eigenfunctions of multiple operators correlates with a higher level of 'homogeneity' of such a set, i.e., the effect of the differences between the individual operators on the inhomogeneous set of eigenstates is smaller. This means that the set $\{\chi_{nl;\beta=1}(r)\}$ more closely represents an array of one-dimensional stationary states of a common operator, i.e., a homogeneous set of eigenfunctions, than the set $\{\zeta_{lm}(\theta)\}$.

The coupling of the r- and θ-dependent components of the H atom eigenstates $\sigma_{nlm;\beta=1}(r, \theta, \phi)$ to the $Y_l^m(\theta, \phi)$ and $\nu_m(\phi)$ factors is manifested in the presence of l- and m-dependent terms in Eqs. (4.18) and (4.21), respectively. We can therefore conclude that the sensitivity of the set $\{\chi_{nl;\beta=1}(r)\}$ to the l-dependent term contributing to the radial operator in Eq. (4.18) is not as pronounced as the sensitivity of the set $\{\zeta_{lm}(\theta)\}$ to the m-dependent term in Eq. (4.21). The more 'homogeneous' nature of set $\{\chi_{nl;\beta=1}(r)\}$ entails that no angular degrees of freedom are necessary to build the decoupled, although still inhomogeneous, set of radial orbitals $\{\widetilde{\chi}_{nl;\beta=1}(r)\}$.

It is not possible, however, to construct linear combinations of the $\zeta_{lm}(\theta)$ functions that would approximately describe a set of one-dimensional eigenfunctions of one shared θ-dependent operator, only the interaction with the ϕ coordinate guarantees assembly of the homogeneous set of eigenstates $\{Y_l^m(\theta, \phi)\}$ of the $\hat{L}^2(\theta, \phi)$ operator. In physical terms this observation can be interpreted as a stronger coupling between the two angular degrees of freedom as compared to the weaker link of the radial coordinate factor to the two angular components in the H atom wave functions $\sigma_{nlm;\beta=1}(r, \theta, \phi)$.

4.4.2. Radial quadrature rule

In order to derive an accurate quadrature rule for the radial degree of freedom, we can either apply the Gram-Schmidt procedure or the Löwdin symmetric orthogonalization [40,41] to transform the set $\{\chi_{nl;\beta}(r)\}$ into an orthonormal set $\{\widetilde{\chi}_{nl;\beta}(r)\}$ for any value of γ and β.

The fact that the linear independence of the set $\{\chi_{nl;\beta}(r)\}$ is conserved if $\gamma \neq 0$, $\beta \neq 1$ is remarkable since Eq. (4.20) only holds for the $\chi_{nl;\beta}(r)$ functions if $\beta = 1$.

The scenario $\gamma \neq 0$ implies a dependence of β on n, l and m, and each element in the set $\{\chi_{nl;\beta}(r)\}$ is an eigenfunction of a particular radial Hamiltonian operator (Eq. (4.18)) which depends both on the $l(l+1)/r^2$ term and on the value of β. The orthonormality property Eq. (4.20) is therefore no longer valid and the VBR overlap matrix of the set $\{\chi_{nl;\beta}(r)\}$ is in this case consequently a full matrix.

If we consider the VBR overlap matrix elements $\langle\widetilde{\lambda}_m(x)|\widetilde{\lambda}_n(x)\rangle$ of an orthonormal set of basis functions $\{\widetilde{\lambda}_m(x)\}$, then a quadrature rule of 'Gaussian accuracy' would ensure that the $\widetilde{\lambda}_m(x)$ functions satisfy the condition of discrete orthonormality for a summation over the grid points [30]. In other words, a quadrature rule is of Gaussian quality if the GFBR approximation to the VBR overlap matrix is exact.

Quadrature rules of Gaussian accuracy have originally been related to orthogonal polynomials, but can be generalized to sets of certain orthogonal non-polynomial functions [32,33,28,1,42,43,29,30]. In these cases, the underlying quadrature rules for orthogonal polynomials

can be recovered through variable substitution.

For the derivation of a quadrature rule for the $\widetilde{\chi}_{nl;\beta}(r)$ functions, we rely on a generalization of the Golub-Welsch algorithm for orthogonal polynomials [44]. Following Refs. [32,33,28,45], we determine in the first step the N nodes x_q of the quadrature grid by diagonalizing the N-dimensional matrix representation of the coordinate operator in terms of non-polynomial basis functions $\widetilde{\lambda}_m(x)$, i.e., the matrix elements are $\langle\widetilde{\lambda}_m(x)|x|\widetilde{\lambda}_n(x)\rangle$. Note that the eigenvalues of the matrix representations of x in terms of the non-orthonormal and orthonormal basis sets $\{\lambda_m(x)\}$ and $\{\widetilde{\lambda}_m(x)\}$, respectively, are not identical because the orthogonalization transformation is not unitary.

In the second step, the N quadrature weights w_q are computed in analogy with the procedure for orthogonal polynomials, by employing Eq. (59) of Ref. [46]:

$$w_q^{-1} = \sum_{m=1}^{N} (\widetilde{\lambda}_m(x_q))^2. \tag{4.25}$$

Application of this two-step scheme yields a quadrature rule for the $\widetilde{\chi}_{nl;\beta}(r)$ functions which is of very high quality both if $\beta = 1$ and if $\beta \neq 1$. However, we find that the orthonormality of the set $\{\widetilde{\chi}_{nl;\beta}(r)\}$ in the VBR is only approximately reproduced in the GFBR, i.e., the set $\{\widetilde{\chi}_{nl;\beta}(r)\}$ does not exactly satisfy the condition of discrete orthonormality and the quadrature prescription is therefore not of Gaussian accuracy.

The $\{\sigma_{nlm;\beta}(r, \theta, \phi)\}$ basis set is composed of the eigenfunctions of $\widehat{\mathscr{H}}_\beta(r, \theta, \phi)$ and can therefore be conveniently employed for the representation of $\widehat{H}_\gamma(r, \theta, \phi)$. The only reason for constructing the $\{\widetilde{\chi}_{nl;\beta}(r)\}$ basis set is therefore the evaluation of the quadrature points r_k and of the corresponding weights $w_{r;k}$.

The quadrature rule derived for the set $\{\widetilde{\chi}_{nl;\beta}(r)\}$ can be directly transferred to the set $\{\chi_{nl;\beta}(r)\}$ without and with minor reduction in accuracy if $\beta = 1$ and if $\beta \neq 1$, respectively (*vide infra*). This can be straightforwardly shown by considering the overlap matrix of a set of non-orthonormal basis functions $\{\lambda_m(x)\}$ which can be transformed into an orthonormal set $\{\widetilde{\lambda}_m(x)\}$. Focussing on one element of the overlap matrix and substituting $\lambda_m(x)$ and $\lambda_n(x)$ through linear expansions in terms of the basis functions in the set $\{\widetilde{\lambda}_m(x)\}$:

$$\lambda_m(x) \coloneqq \sum_{k=1}^{N} c_{mk}\widetilde{\lambda}_k(x), \tag{4.26}$$

we get

$$\begin{aligned}\int \lambda_m(x)\lambda_n(x)\mathrm{d}x &= \int \left(\sum_{j=1}^{N} c_{mj}\widetilde{\lambda}_j(x)\right)\left(\sum_{k=1}^{N} c_{nk}\widetilde{\lambda}_k(x)\right)\mathrm{d}x \\ &= \sum_{j=1}^{N}\sum_{k=1}^{N} c_{nk}c_{mj}\int \widetilde{\lambda}_j(x)\widetilde{\lambda}_k(x)\mathrm{d}x \\ &= \sum_{j=1}^{N}\sum_{k=1}^{N} c_{mj}c_{nk}\delta_{jk} = \sum_{j=1}^{N} c_{mj}c_{nj},\end{aligned} \tag{4.27}$$

$$\int \widetilde{\lambda}_j(x)\widetilde{\lambda}_k(x)\mathrm{d}x = \delta_{jk} \approx \sum_{q=1}^{N} w_q\widetilde{\lambda}_j(x_q)\widetilde{\lambda}_k(x_q), \tag{4.28}$$

where c_{mk} denotes an expansion coefficient obtained by Gram-Schmidt or Löwdin orthogonalization.

Eqs. (4.27) and (4.28) demonstrate that a quadrature approximation to $\int \lambda_j(x)\lambda_k(x)\mathrm{d}x$ using the weights w_q and grid points x_q depends on the accuracy of the discrete orthonormality relation of $\widetilde{\lambda}_j(x)$ and $\widetilde{\lambda}_k(x)$. As mentioned above, the discrete orthonormality condition is closely, but not exactly, satisfied by the set $\{\widetilde{\chi}_{nl;\beta}(r)\}$. This is true for all values of β. In order to assess the quality of the radial quadrature rule for the set $\{\chi_{nl;\beta}(r)\}$, we nevertheless need to differentiate between the cases $\beta = 1$ and $\beta \neq 1$, because quadrature rules of Gaussian accuracy for the numerical evaluation of matrix elements demand orthogonality of basis functions in the VBR (cf. Section 4.4.1). The quadrature prescription outlined in this section can accordingly reach near Gaussian accuracy for GFBR matrix elements of local operators between $\chi_{nl;\beta}(r)$ functions with common index l only if $\beta = 1$ and will be of lower quality if $\beta \neq 1$ due to the invalidity of the orthogonality property Eq. (4.20) in this case. For the evaluation of these matrix elements, the quadrature rule (grid points r_k, weights $w_{r;k}$) defined for the set $\{\widetilde{\chi}_{nl;\beta}(r)\}$ can therefore only be applied to the set $\{\chi_{nl;\beta}(r)\}$ at the same level of quality if $\beta = 1$.

4.4.3. Derivation of angular quadrature rule

We now proceed to a discussion of the quadrature rule for the two angular variables, θ and ϕ. The coupling of the θ and ϕ coordinates in the $Y_l^m(\theta, \phi)$ functions implies that the computation of the diagonal VBR overlap matrix of the set $\{Y_l^m(\theta, \phi)\}$ is intrinsically a two-dimensional problem. If both sets $\{\zeta_{lm}(\theta)\}$ and $\{\nu_m(\phi)\}$ were orthonormal, collecting the diagonal elements of the overlap matrices of both sets would provide all the information needed for the evaluation of the overlap matrix of the set $\{Y_l^m(\theta, \phi)\}$. However, the full overlap matrix of the set $\{\zeta_{lm}(\theta)\}$ needs to be considered for the calculation of the overlap matrix of the set $\{Y_l^m(\theta, \phi)\}$ because the θ-dependent components cannot be orthonormalized, as described in Section 4.4.1.

The orthonormality of the set $\{\nu_m(\phi)\}$ ensures that the non-zero off-diagonal elements of the overlap matrix of the set $\{\zeta_{lm}(\theta)\}$ do not induce any non-zero off-diagonal entries in the overlap matrix of the set $\{Y_l^m(\theta, \phi)\}$. This feature underscores the non-separability of the θ and ϕ degrees of freedom in the $Y_l^m(\theta, \phi)$ functions, which becomes evident also in the discrete orthonormality relation for the set $\{Y_l^m(\theta, \phi)\}$.

Various attempts have been made at formulating a quadrature rule for the $Y_l^m(\theta, \phi)$ functions [47,45,48]. Ref. [47] suggests two formulations which differ with respect to the lattice required for a discrete orthonormality of the set $\{Y_l^m(\theta, \phi)\}$: (i) a grid uniform in $\cos(\theta)$ and ϕ and (ii) a grid uniform in θ and ϕ. We use option (i) and, following Ref. [47], make use of relations between families of orthogonal polynomials or, more generally, of orthogonal functions. Spherical harmonics are usually defined as a product of Fourier and associated Legendre functions $P_l^m(x)$. However, the classical orthogonal polynomials [49] can all be derived from Jacobi polynomials $P_l^{(\rho,\tau)}(x)$ [50] and also the associated Legendre functions are related to Jacobi polynomials [51] through:

$$\begin{aligned}(-1)^m P_l^m(x) &= (-1)^m \tfrac{(l+1)!}{(l+1-m)!}\tfrac{1}{2^m}\sqrt{w_J(x)}\,P_{l-m}^{(m,m)}(x), \\ w_J(x) &\coloneqq (1-x^2)^m,\end{aligned} \tag{4.29}$$

where $w_J(x)$ is the weight function for $P_{l-m}^{(m,m)}(x)$.

In order to define a quadrature rule for the spherical harmonics, we make two substitutions of the θ-dependent component of $Y_l^m(\theta, \phi)$: in the first step, the associated Legendre functions are rewritten in terms of Jacobi polynomials according to Eq. (4.29). In the next step, we use the asymptotic relation [47] that connects the Hahn polynomial $h_l^{(\rho,\tau)}(s, N_\theta)$ and Jacobi polynomial $P_l^{(\rho,\tau)}(x)$, where $x \coloneqq \cos(\theta)$ and $s \coloneqq \overline{N}_\theta(1 + x)/2 - (\tau + 1)/2$, $\overline{N}_\theta \coloneqq N_\theta + (\rho + \tau)/2$. The variable transformation $x \to s$ corresponds to an adaptation of the definition interval [-1, 1] for $P_l^{(\rho,\tau)}(x)$ to the definition interval [0, N_θ] for $h_l^{(\rho,\tau)}(s, N_\theta)$. The discrete variable s is represented by the vector $(s_1, s_2, ..., s_{N_\theta})^T$ with grid spacing $\Delta s \coloneqq 2/N_\theta$. The Hahn polynomials are thus the discrete analogs of the Jacobi polynomials. They are orthogonal on an equidistant N_θ-point lattice in the interval [0, N_θ - 1] when $\rho > -1$ and $\tau > -1$ [47,52,53].

In the limit $\overline{N}_\theta \to \infty$, the discrete variable s becomes continuous and the functions $h_l^{(m,m)}(s, N_\theta)$ and $\bar{w}_J(s)$ converge to $P_l^{(m,m)}(x)$ and $w_J(x)$,

respectively. This allows us to make the following identification:

$$\xi_{lm}\sqrt{w_J(x)}P_l^{(m,m)}(x) = \frac{\bar{\xi}_{lm}\sqrt{\bar{w}_J(s)}}{\sqrt{\Delta x}}h_l^{(m,m)}(s, N_\theta) + O\left(\frac{1}{\overline{N}_\theta^2}\right), \tag{4.30}$$

$$s = \frac{\overline{N}_\theta}{2}(1+x) - \frac{m+1}{2},\ \overline{N}_\theta = N_\theta - m,\ \Delta x = \frac{2}{\overline{N}_\theta}, \tag{4.31}$$

where ξ_{lm} and $\bar{\xi}_{lm}$ are normalization factors for $P_l^{(m,m)}(x)$ and $h_l^{(m,m)}(s, N_\theta)$, respectively, $\bar{w}_J(s)$ is the weight function for $h_l^{(m,m)}(s, N_\theta)$ and the notation $O(1/\overline{N}_\theta^2)$ implies that the size of this term is of the order of $1/\overline{N}_\theta^2$.

The substitution of the Jacobi polynomials of continuous argument x by the Hahn polynomials of discrete variable s is the key step in deriving a quadrature rule for the spherical harmonics. The functions $\overline{Y}_l^m(\theta, \phi)$ are approximations to the spherical harmonics $Y_l^m(\theta, \phi)$:

$$\begin{aligned}\overline{Y}_l^m(\theta, \phi) &:= \sqrt{2\pi}\sqrt{\frac{(2l+1)(l-m)!}{4\pi(l+m)!}}\frac{(l+1)!}{(l+1-m)!}\times \\ &\frac{1}{2^m}\frac{\sqrt{\bar{w}_J(s)}}{\sqrt{\Delta x}}h_{l-m}^{(m,m)}(s, N_\theta)\nu_m(\phi)\ \ (m \geqslant 0), \\ \overline{Y}_l^{-m}(\theta, \phi) &= (-1)^m(\overline{Y}_l^m(\theta, \phi))^*,\end{aligned} \tag{4.32}$$

and have the property of discrete orthogonality:

$$\sum_{i=0}^{\overline{N}_\theta - m - 1}\sum_{j=0}^{N_\phi - 1}\overline{Y}_l^m(\theta_{im}, \phi_j)(\overline{Y}_{l'}^{m'}(\theta_{im'}, \phi_j))^*\Delta x\,\Delta\phi = \delta_{ll'}\delta_{mm'}, \tag{4.33}$$

where

$$\begin{aligned}\cos(\theta_{im}) = x_{2i+m+1},\ x_k &= -1 + \frac{k}{\overline{N}_\theta}\ \ (i = 0, 1, \ldots, \overline{N}_\theta - m - 1), \\ \phi_j &= -\pi + \frac{\pi}{N_\phi}(2j+1)\ \ (j = 0, 1, \ldots, N_\phi - 1), \\ \Delta\phi &= \frac{2\pi}{N_\phi}.\end{aligned} \tag{4.34}$$

We finally obtain an approximate discrete orthonormality relation for the set $\{Y_l^m(\theta, \phi)\}$:

$$\begin{aligned}&\sum_{j=0}^{{}^{\mathrm{GFBR}}N_\theta - m - 1}\sum_{k=0}^{{}^{\mathrm{GFBR}}N_\phi - 1}\zeta_{lm}(\theta_{jm})\nu_m(\phi_k)(\nu_{m'}(\phi_k))^*\zeta_{l'm'}(\theta_{jm'})\,{}^{\mathrm{GFBR}}\Delta x\,{}^{\mathrm{GFBR}}\Delta\phi \\ &= \sum_{j=0}^{{}^{\mathrm{GFBR}}N_\theta - m - 1}\zeta_{lm}(\theta_{jm})\zeta_{l'm}(\theta_{jm})\,{}^{\mathrm{GFBR}}\Delta x\,\delta_{mm'} \approx \delta_{ll'}\delta_{mm'},\end{aligned} \tag{4.35}$$

where

$$\cos(\theta_{jm}) = x_{2j+m+1},\ x_a = -1 + \frac{a}{{}^{\mathrm{GFBR}}N_\theta}\ \ (j = 0, 1, \ldots, {}^{\mathrm{GFBR}}N_\theta - m - 1), \tag{4.36}$$

$$\phi_k = -\pi + \frac{\pi}{{}^{\mathrm{GFBR}}N_\phi}(2k+1)\ \ (k = 0, 1, \ldots, {}^{\mathrm{GFBR}}N_\phi - 1), \tag{4.37}$$

$${}^{\mathrm{GFBR}}\Delta x = \frac{2}{{}^{\mathrm{GFBR}}N_\theta}, \tag{4.38}$$

$${}^{\mathrm{GFBR}}\Delta\phi = \frac{2\pi}{{}^{\mathrm{GFBR}}N_\phi}. \tag{4.39}$$

According to Eq. (4.33), the quadrature rule Approx. 4.35 becomes exact for ${}^{\mathrm{GFBR}}N_\theta \to \infty$, i.e., this limit corresponds to Gaussian accuracy. As an important distinction compared to the discrete orthonormality relation for the set $\{\widetilde{\chi}_{nl;\beta}(r)\}$, which is only approximately satisfied, we note that the grid dimensions ${}^{\mathrm{GFBR}}N_\theta$ and ${}^{\mathrm{GFBR}}N_\phi$ can be defined without restrictions, i.e., ${}^{\mathrm{GFBR}}N_\theta$ may also differ from ${}^{\mathrm{GFBR}}N_\phi$, whereas N_r is linked to n_{max}. Because of the method used for the computation of r_k, the size N_r of the radial grid $\{r_k\}$ must be identical to the number of radial basis functions $\chi_{nl;\beta}(r)$, which depends on n_{max}. However, Eqs. (4.36) and (4.37) show that the dimensions ${}^{\mathrm{GFBR}}N_\theta$ and ${}^{\mathrm{GFBR}}N_\phi$ of the quadrature lattice in the direction of the θ and ϕ coordinates, respectively, are decoupled from the n_{max}-dependent sizes ${}^{\mathrm{VBR}}N_\theta$ and ${}^{\mathrm{VBR}}N_\phi$ of the sets $\{\zeta_{lm}(\theta)\}$ and $\{\nu_m(\phi)\}$, respectively.

4.4.4. Evaluation of GFBR matrix elements of $\widehat{H}_{loc}$ and of general local operators

The definition of quadrature rules for the radial and angular components in Sections 4.4.2 and 4.4.3, respectively, allows for the formulation of an approximate discrete orthonormality relation for the eigenfunctions $\sigma_{nlm;\beta}(r, \theta, \phi)$ of $\widehat{\mathscr{H}}_\beta(r, \theta, \phi)$:

$$\begin{aligned}&\int_0^\infty r^2\mathrm{d}r\int_0^\pi \sin(\theta)\mathrm{d}\theta\int_0^{2\pi}\mathrm{d}\phi\ \sigma_{nlm;\beta}(r, \theta, \phi)(\sigma_{n'l'm';\beta'}(r, \theta, \phi))^* = \\ &\int_0^\infty r^2\mathrm{d}r\int_0^\pi \sin(\theta)\mathrm{d}\theta\int_0^{2\pi}\mathrm{d}\phi\ \chi_{nl;\beta}(r)\zeta_{lm}(\theta)\nu_m(\phi)(\nu_{m'}(\phi))^*\zeta_{l'm'}(\theta)\chi_{n'l';\beta'}(r) \\ &\left.\begin{cases} = & (\text{if } \beta = \beta' = 1) \\ \approx & (\text{if } \beta, \beta' \neq 1)\end{cases}\right\}\delta_{nn'}\delta_{ll'}\delta_{mm'} \approx \\ &\sum_{i=1}^{N_r}\sum_{j=0}^{{}^{\mathrm{GFBR}}N_\theta - m - 1}\sum_{k=0}^{{}^{\mathrm{GFBR}}N_\phi - 1}w_{r;i}\,{}^{\mathrm{GFBR}}\Delta x\,{}^{\mathrm{GFBR}}\Delta\phi\times \\ &\chi_{nl;\beta}(r_i)\zeta_{lm}(\theta_{jm})\nu_m(\phi_k)(\nu_{m'}(\phi_k))^*\zeta_{l'm'}(\theta_{jm'})\chi_{n'l';\beta'}(r_i) = \\ &\left(\sum_{i=1}^{N_r}\sum_{j=0}^{{}^{\mathrm{GFBR}}N_\theta - m - 1}w_{r;i}\,{}^{\mathrm{GFBR}}\Delta x\,\chi_{nl;\beta}(r_i)\zeta_{lm}(\theta_{jm})\zeta_{l'm'}(\theta_{jm'})\chi_{n'l';\beta'}(r_i)\right) \\ &\times\left(\sum_{k=0}^{{}^{\mathrm{GFBR}}N_\phi - 1}{}^{\mathrm{GFBR}}\Delta\phi\ \nu_m(\phi_k)(\nu_{m'}(\phi_k))^*\right) = \\ &\left(\sum_{i=1}^{N_r}\sum_{j=0}^{{}^{\mathrm{GFBR}}N_\theta - m - 1}w_{r;i}\,{}^{\mathrm{GFBR}}\Delta x\,\chi_{nl;\beta}(r_i)\zeta_{lm}(\theta_{jm})\zeta_{l'm}(\theta_{jm})\chi_{n'l';\beta'}(r_i)\right)\delta_{mm'} = \\ &\left(\sum_{i=1}^{N_r}w_{r;i}\chi_{nl;\beta}(r_i)\chi_{n'l';\beta'}(r_i)\right)\left(\sum_{j=0}^{{}^{\mathrm{GFBR}}N_\theta - m - 1}{}^{\mathrm{GFBR}}\Delta x\,\zeta_{lm}(\theta_{jm})\zeta_{l'm}(\theta_{jm})\right)\delta_{mm'} \approx \\ &\left(\sum_{i=1}^{N_r}w_{r;i}\chi_{nl;\beta}(r_i)\chi_{n'l';\beta'}(r_i)\right)\delta_{ll'}\delta_{mm'} \approx \delta_{nn'}\delta_{ll'}\delta_{mm'}\end{aligned} \tag{4.40}$$

The quality of the last approximation, i.e., the assumption of discrete orthonormality of the $\chi_{nl;\beta}(r)$ and $\chi_{n'l;\beta'}(r)$ functions, depends on the values of β and β': $\beta = \beta' = 1$ means that the orthormality relation Eq. (4.20) holds and that the highest accuracy of the corresponding discrete orthonormality formula can be reached. The more β differs from β', the lower the quality of the discrete orthonormality approximation will be.

VBR matrix elements of a general, nonseparable local operator $\widehat{O}_{loc}(r, \theta, \phi)$ can be approximated in the GFBR as:

$$\begin{aligned}&\int_0^\infty r^2\mathrm{d}r\int_0^\pi \sin(\theta)\mathrm{d}\theta\int_0^{2\pi}\mathrm{d}\phi\ \chi_{nl;\beta}(r)\zeta_{lm}(\theta)\nu_m(\phi)\widehat{O}_{loc}(r, \theta, \phi)\times \\ &(\nu_{m'}(\phi))^*\zeta_{l'm'}(\theta)\chi_{n'l';\beta'}(r) \approx \\ &\sum_{i=1}^{N_r}\sum_{j=0}^{{}^{\mathrm{GFBR}}N_\theta - m - 1}\sum_{k=0}^{{}^{\mathrm{GFBR}}N_\phi - 1}w_{r;i}\,{}^{\mathrm{GFBR}}\Delta x\,{}^{\mathrm{GFBR}}\Delta\phi\times \\ &\chi_{nl;\beta}(r_i)\zeta_{lm}(\theta_{jm})\nu_m(\phi_k)\widehat{O}_{loc}(r_i, \theta_{jm}, \phi_k)(\nu_{m'}(\phi_k))^*\zeta_{l'm'}(\theta_{jm'})\chi_{n'l';\beta'}(r_i)\end{aligned} \tag{4.41}$$

Evaluation of a GFBR of operator $\widehat{H}_{loc}$ is greatly simplified compared to Approx. 4.41 for GFBR matrix elements of operator $\widehat{O}_{loc}(r, \theta, \phi)$ because the ϕ coordinate can be separated, leading to a sparse, but not block-diagonal, structure of the GFBR of $\widehat{H}_{loc}$:

$$\int_0^\infty r^2 \mathrm{d}r \int_0^\pi \sin(\theta)\mathrm{d}\theta \int_0^{2\pi} \mathrm{d}\phi\, \chi_{nl;\beta}(r)\zeta_{lm}(\theta)\nu_m(\phi)\widehat{H}_{loc}\times (\nu_{m'}(\phi))^*\zeta_{l'm'}(\theta)\chi_{n'l';\beta'}(r) \approx$$

$$\sum_{i=1}^{N_r} \sum_{j=0}^{{}^{\mathrm{GFBR}}N_\theta - m - 1} \sum_{k=0}^{{}^{\mathrm{GFBR}}N_\phi - 1} w_{r;i}\, {}^{\mathrm{GFBR}}\Delta x\, {}^{\mathrm{GFBR}}\Delta\phi \times \chi_{nl;\beta}(r_i)\zeta_{lm}(\theta_{jm})\nu_m(\phi_k)\left(\widehat{V}_H(r_i) + \frac{\gamma^2}{8\mu} r_i^2 (\sin(\theta_{jm}))^2\right)\times (\nu_{m'}(\phi_k))^*\zeta_{l'm'}(\theta_{jm'})\chi_{n'l';\beta'}(r_i) =$$

$$\left(\sum_{k=0}^{{}^{\mathrm{GFBR}}N_\phi - 1} {}^{\mathrm{GFBR}}\Delta\phi\ \nu_m(\phi_k)(\nu_{m'}(\phi_k))^*\right)\times \left(\sum_{i=1}^{N_r} \sum_{j=0}^{{}^{\mathrm{GFBR}}N_\theta - m - 1} w_{r;i}\, {}^{\mathrm{GFBR}}\Delta x\, \chi_{nl;\beta}(r_i)\zeta_{lm}(\theta_{jm})\left(\widehat{V}_H(r_i) + \frac{\gamma^2}{8\mu} r_i^2 (\sin(\theta_{jm}))^2\right)\zeta_{l'm'}(\theta_{jm'})\chi_{n'l';\beta'}(r_i)\right) =$$

$$\left(\sum_{i=1}^{N_r} \sum_{j=0}^{{}^{\mathrm{GFBR}}N_\theta - m - 1} w_{r;i}\, {}^{\mathrm{GFBR}}\Delta x\, \chi_{nl;\beta}(r_i)\zeta_{lm}(\theta_{jm})\left(\widehat{V}_H(r_i) + \frac{\gamma^2}{8\mu} r_i^2 (\sin(\theta_{jm}))^2\right)\zeta_{l'm}(\theta_{jm})\chi_{n'l';\beta'}(r_i)\right)\delta_{mm'} \tag{4.42}$$

5. Computational results

5.1. The field-free H atom: Investigation of angular quadrature convergence and comparison of VBR vs. GFBR performance

We first focus on the field-free H atom ($\gamma = 0, \beta = 1$) and compare in Table 1 the energies of states for $n = 1, 2, 3$ obtained with the Hamiltonians $\mathbf{H}_1$ (VBR, Def. 3.1) and $\mathbf{H}_2$ (GFBR, Def. 3.2). This is the case where the highest possible accuracy of the GFBR approach can be obtained since the set $\{\sigma_{nlm;\beta}(r, \theta, \phi)\}$ in this case can be made orthonormal (cf. Sections 4.4.1 and 4.4.2). As we limit ourselves to states with $n \leqslant 3$, the dimension ${}^{\mathrm{VBR}}N$ of $\mathbf{H}_1$ is fully determined by the highest value for n, giving $N_r = 6$, ${}^{\mathrm{VBR}}N_\theta = 9$ and ${}^{\mathrm{VBR}}N_\phi = 5$, leading to ${}^{\mathrm{VBR}}N = 14$ (cf. Section 4.1).

The sizes of the matrices $\mathbf{H}_1$ and $\mathbf{H}_2$ are identical, but the computation of the local component ${}^{\mathrm{GFBR}}\mathbf{H}_{loc}$ of $\mathbf{H}_2$ requires in addition information (provided in Table 1) on ${}^{\mathrm{GFBR}}N_\phi$ and ${}^{\mathrm{GFBR}}N_\theta$, the numbers defining the angular quadrature grid (cf. Section 4.4.3). The radial lattice has N_r points. With these parameters, the quadrature approximation ${}^{\mathrm{GFBR}}\mathbf{H}_{loc}$ to ${}^{\mathrm{VBR}}\mathbf{H}_{loc}$ can be considered nearly converged with respect to the angular degrees of freedom (cf. Fig. 2 and the discussion below). However, N_r is too small to reach a full radial convergence of the matrix elements of ${}^{\mathrm{GFBR}}\mathbf{H}_{loc}$. We nevertheless decide to accept this deficiency because N_r, unlike ${}^{\mathrm{GFBR}}N_\phi$ and ${}^{\mathrm{GFBR}}N_\theta$, is tied to n_{max} (cf. Section 4.4.3) and we prefer to restrict the states of interest, and thus also the basis set $\{\sigma_{nlm;\beta}(r, \theta, \phi)\}$, to $n = 1, 2, 3$ in the present study.

In future work we will also investigate quadrature convergence with respect to the radial coordinate. We recall that the set $\{\chi_{nl;\beta}(r)\}$ is linearly independent. However, the construction of the orthonormal set $\{\widetilde{\chi}_{nl;\beta}(r)\}$ becomes increasingly more difficult with increasing n_{max}. We prefer Löwdin symmetric orthogonalization [40,41] over the Gram-Schmidt procedure and while double-precision arithmetic is sufficient to resolve linear independence for a radial basis size up to $n_{max} = 4$, quadruple precision is required when the maximum value of n is 5 since the smallest eigenvalue of the overlap matrix of the set $\{\chi_{nl;\beta=1}(r)\}$ in this case is of the order 10^{-25}.

Fig. 1 shows the distribution of the radial grid points for the sets $\{r_k\}$ with maximum $n = 3, 4, 5$. The basis set $\{\chi_{nl;\beta=1}(r)\}$ has been employed for the computation of the three radial lattices. It can be seen that the range covered by the grid points is loosely correlated to the expectation values $\langle r \rangle$ of the radial components of the field-free H atom wave functions. The ratios between the values of the grid points with the maximum distance from the nucleus ($n_{max} = 3 \rightarrow 22.075\ a_0$, $n_{max} = 4 \rightarrow 50.141\ a_0$, $n_{max} = 5 \rightarrow 93.381\ a_0$) and $\langle r \rangle$ for the radial factors of 3s (7.144 a_0), 4s (12.700 a_0) and 5s (19.844 a_0) H atom eigenfunctions [54] are 3.09, 3.95 and 4.70, respectively, all being of the same order of magnitude.

Inspection of Table 1 reveals that the quality of the GFBR approximations shows a clear trend: eigenvalues of $l = 0$ states are significantly less accurate than those of $l > 0$ states. Whereas the calculated energies for $l > 0$ show a consistent and high precision, we note a strong decrease in the quality of the description of the $l = 0$ states with smaller values of n. Interestingly, the GFBR energies of Table 1 are consistently higher than the corresponding VBR estimates. This is not an implicit property of GFBR predictions because of the non-variational nature of this method, as can be seen from Tables 2, 4 and 5.

There are two main reasons for the large accuracy bandwidth of the GFBR electronic energy estimates of Table 1: (i) The amplitude of the exact radial probability densities $4\pi r^2(\chi_{nl;\beta=1}(r))^2$ of the states. Obviously, the representation of sharply peaked densities on such a sparse radial grid is problematic. (ii) The number and position of the nodes is also critical for the accuracy of the quadrature approximation. A proper description of a nodal region requires a dense support mesh.

A comparison of the relevant radial probability densities shows that the density of the 1s state is quite narrow and has a maximum near $1a_0$, the 2s and 2p densities both peak near $5a_0$ and the 3s, 3p and 3d densities reach their global extrema at about $13a_0$, $12a_0$ and $9a_0$, respectively. The 1s, 2s and 3s densities are characterized by zero, one and two nodes, respectively.

Since $l = 0$ wave functions do not depend on θ and ϕ, they are described by the radial component alone. The difference in the GFBR accuracy of the 1s, 2s and 3s energies reflects the structure of the $\{r_k\}$ lattice: the distribution of grid points allows for a much better representation of the broader 2s and in particular 3s densities than of the 1s density which is sharply peaked near the nucleus. Only two grid points (r_1, r_2) are sufficiently close to the maximum to recover the contribution to the 1s density coming from this region. The width of the radial density dominates the quality of the approximation for $l = 0$ states since the quadrature error does not increase with increasing number of nodes in the radial wave function.

The spread of the radial probability densities does not explain why the GFBR energies for $l > 0$ are about an order of magnitude more accurate than those for $l = 0$ for $n = 2$ and $n = 3$. We recall that for $l > 0$, the eigenstates are functions of both r and either θ or both angles.

The real spherical harmonics of $l = 1$ and $l = 2$ states are characterized by nodes at the nucleus, and this topology needs to be superimposed on the radial density in order to obtain the three-

Table 1
Energies (in a. u.) of states of the field-free H atom ($\gamma = 0, \beta = 1$) with $n = 1, 2, 3$ are shown. Eigenvalues of Hamiltonian constructions $\mathbf{H}_1$ (VBR, Def. 3.1) and $\mathbf{H}_2$ (GFBR, Def. 3.2) are included. For each state, the fractional error of the GFBR approximation relative to the VBR result is provided. Quadrature parameters employed for the computation of matrix elements of the local component ${}^{\mathrm{GFBR}}\mathbf{H}_{loc}$ of $\mathbf{H}_2$: $N_r = 6$, ${}^{\mathrm{GFBR}}N_\phi = 15$ and ${}^{\mathrm{GFBR}}N_\theta = 15$.

State	Calculated Energy		Fractional Error
	VBR	GFBR	|E(GFBR)−E(VBR)|/E(VBR)
1s	−0.5000	−0.3613	0.2774
2s	−0.1250	−0.1056	0.1552
$2p_{-1,0,1}$	−0.1250	−0.1215	0.0280
3s	−0.0556	−0.0495	0.1097
$3p_{-1,0,1}$	−0.0556	−0.0541	0.0270
$3d_{-2,-1,0,1,2}$	−0.0556	−0.0540	0.0288

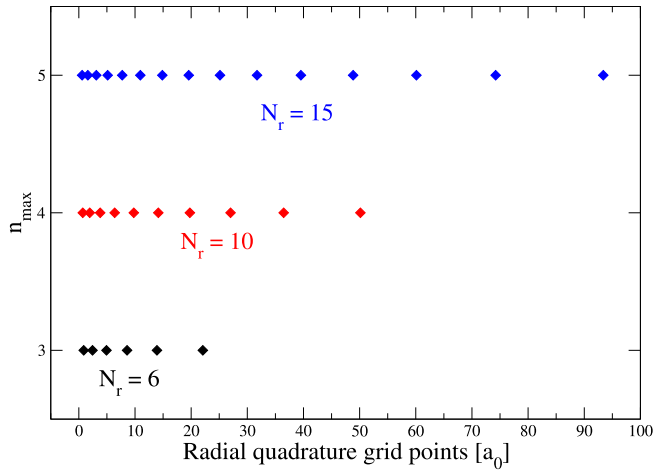

Fig. 1. The structures of radial grids $\{r_k\}$ obtained by the method described in Section 4.4.2 are shown for maximum values of $n = 3, 4, 5$ corresponding to grid sizes $N_r = 6, 10, 15$. The set of radial components $\{\chi_{nl;\beta=1}(r)\}$ of field-free H atom eigenfunctions has been employed for the calculation of the three grids. Only the radial grid with $N_r = 6$ has been applied for the GFBR calculations reported in this work.

dimensional probability density. As the total number of nodes is fixed for a given value of n, the nuclear node of $l > 0$ spherical harmonics implies that the radial probability densities of the corresponding states have l nodes less than the radial densities of $l = 0$ states. This lowers the demands on the radial wave function to describe the nodal structure, leading to much lower GFBR errors for states with $l > 0$. We conclude that the extra node of the 2*s* radial density is mainly responsible for the larger error of the GFBR energy as compared to the 2*p* state. Analogously, the appearance of one and two additional nodes in the 3*s* radial density accounts for the more precise GFBR description of the 3*p* and 3*d* states, respectively.

Let us finally address the slightly higher accuracy of the 3*p* vs. the 3*d* energy: only the 3*p* radial density features a node for $r > 0$ and is therefore more spread out than the 3*d* density, better matching the structure of the grid than the 3*d* density, compensating for the challenge imposed by the quadrature approximation of the node.

The results shown in Fig. 2 are also based on the orthonormal $\{\sigma_{nlm;\beta=1}(r, \theta, \phi)\}$ basis set. Fig. 2 depicts the convergence properties of the GFBR energies of the 1*s*, 2*s* and 2*p* states of the field-free H atom with respect to the angular grid dimensions ${}^{\mathrm{GFBR}}N_\phi$ and ${}^{\mathrm{GFBR}}N_\theta$. A GFBR calculation with $N_r = 6$ and ${}^{\mathrm{GFBR}}N_\phi = {}^{\mathrm{GFBR}}N_\theta = 30$ provides the reference energies. ${}^{\mathrm{GFBR}}N_\phi$ and ${}^{\mathrm{GFBR}}N_\theta$ are increased symmetrically from 5 to 30 with increments of 5 and a GFBR calculation is performed for each lattice. The dependence of the differences between the resulting 1*s*, 2*s* and 2*p* energies and the reference values on the angular lattice sizes is shown in Fig. 2. It can be seen that the accuracy of the GFBR description improves nearly linearly and convergence is reached at ca. 30.

5.2. The H atom in a uniform magnetic field: Comparison of VBR and GFBR

In Table 2, we report the energies of selected states of the H atom in a uniform magnetic field ($\gamma = 0.1$) calculated with different methods. In the table, we also compare to results of Ref. [26].

Both the calculations performed for Table I of Ref. [26] and for Table 2 relied either on the non-optimized ($\{\sigma_{nlm;\beta=1}(r, \theta, \phi)\}$) or the optimized ($\{\sigma_{nlm;\beta}(r, \theta, \phi)\}$) basis set. The energies compiled in Table I of Ref. [26] that have been obtained with $\sigma_{nlm;\beta=1}(r, \theta, \phi)$ basis functions correspond to first-order perturbation theory calculations. The β values for the $\{\sigma_{nlm;\beta}(r, \theta, \phi)\}$ basis set optimized for the magnetic field strength $\gamma = 0.1$ can be found in Table 3. The results of Table 2 reveal that first-order perturbation theory is quite accurate for $l = 0$ and $l = 1$ states, but fails completely for $l = 2$ states.

The calculations summarized in columns 4 and 5 of Table 2 have been performed with the VBR and GFBR methods, respectively, employing field-free H atom eigenfunctions as a basis set ($\{\sigma_{nlm;\beta=1}(r, \theta, \phi)\}$). The similarity between the results of columns 2 and 4 demonstrates that the variational flexibility introduced by an expansion in terms of the $\{\sigma_{nlm;\beta=1}(r, \theta, \phi)\}$ basis functions only leads to a minor improvement in the VBR accuracy relative to the non-variational version of the one-basis-function-per-state approach of Ref. [26]. The linear combinations of the basis functions thus do not appear to describe the eigenfunctions of this system well.

A comparison of the results reported in columns 4 and 5 of Table 2 provides evidence that the GFBR approach in combination with the $\{\sigma_{nlm;\beta=1}(r, \theta, \phi)\}$ basis set yields a good approximation to the corresponding VBR energies of the 2*s*, $3d_{-1}$ and $3d_{-2}$ states, whereas the VBR

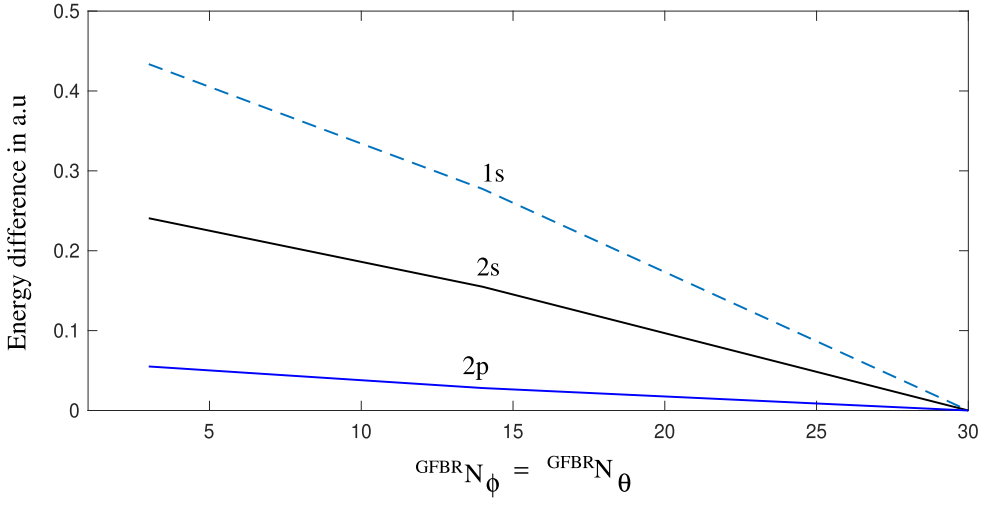

Fig. 2. Convergence of the GFBR energies of the 1*s*, 2*s* and 2*p* states of the field-free H atom ($\gamma = 0, \beta = 1$) with respect to the number of grid points representing each angular degree of freedom. In all calculations, the number N_r corresponding to the radial lattice dimension is fixed at 6 and identical GFBR grid sizes are employed for both angular coordinates: ${}^{\mathrm{GFBR}}N_\phi = {}^{\mathrm{GFBR}}N_\theta$. The following numbers (marked on the abscissa) define the dimension of the angular quadrature lattice in the direction of each angle: 5, 10, 15, 20, 25, 30. The largest grid is described by $N_r = 6$, ${}^{\mathrm{GFBR}}N_\phi = {}^{\mathrm{GFBR}}N_\theta = 30$ and the eigenvalues of Hamiltonian construction $\mathbf{H}_2$ (GFBR, Def. 3.2) computed with these quadrature parameters provide the reference energies of the 1*s*, 2*s* and 2*p* states. For each specified lattice, the eigenvalues of $\mathbf{H}_2$ are then evaluated and the absolute values of the deviations (in a. u.) of the resulting 1*s*, 2*s* and 2*p* energies from the reference values are plotted.

Table 2
Energies (in a. u.) of states of the H atom in a uniform magnetic field ($B = 2.35 \times 10^8 G$, $\gamma = 0.1$) with $n = 1, 2, 3$ are shown. The values listed in columns 2 and 3 are taken from Table I of Ref. [26]. The column 2 and 3 results correspond to first order perturbation theory ($\beta = 1$ case) and to variational optimization of β, respectively. Eigenvalues of Hamiltonian constructions $\mathbf{H}_1$ (VBR, Def. 3.1) and $\mathbf{H}_2$ (GFBR, Def. 3.2) are included. Two basis sets have been employed: (i) the set $\{\sigma_{nlm;\beta=1}(r, \theta, \phi)\}$ corresponds to eigenfunctions of the field-free H atom and (ii) the set $\{\sigma_{nlm;\beta}(r, \theta, \phi)\}$ features functions with variationally optimized β parameter. For each state, the fractional error of the GFBR approximation relative to the VBR result is provided (optimized β only). Quadrature parameters employed for the computation of matrix elements of the local component ${}^{\mathrm{GFBR}}\mathbf{H}_{loc}$ of $\mathbf{H}_2$: $N_r = 6$, ${}^{\mathrm{GFBR}}N_\phi = 15$ and ${}^{\mathrm{GFBR}}N_\theta = 15$.

State	Energies from Ref. [26]		This study				Fractional Error
	First order perturbation theory ($\beta = 1$)	Optimized β	$\beta = 1$		Optimized β		Optimized β
			VBR	GFBR	VBR	GFBR	|E(GFBR)−E(VBR)|/E(VBR)
$1s$	−0.497500	−0.497512	−0.4975	−0.3624	−0.4975	−0.3957	0.2046
$2s$	−0.090000	−0.095882	−0.0900	−0.0898	−0.0958	−0.0749	0.2182
$2p_0$	−0.100000	−0.111363	−0.1100	−0.1700	−0.1114	−0.1101	0.0117
$2p_{-1}$	−0.145000	−0.149509	−0.1450	−0.2095	−0.1488	−0.1470	0.0121
$3d_{-1}$	−0.015556	−0.051678	−0.0156	−0.0145	−0.0515	−0.0503	0.0233
$3d_{-2}$	−0.020556	−0.082822	−0.0206	−0.0209	−0.0800	−0.0792	0.0100

Table 3
Values of the shielding parameter β for electronic states and magnetic field strengths γ relevant to Tables 2 and 4 are provided. The β values have been computed according to Ref. [26].

	State									
γ	$1s$	$2s$	$2p_0$	$2p_{\pm 1}$	$3s$	$3p_0$	$3p_{\pm 1}$	$3d_0$	$3d_{\pm 1}$	$3d_{\pm 2}$
0.0425	1.0009	1.0444	1.0204	1.0387	1.2723	1.1787	1.2794	1.1573	1.1787	1.2337
0.1	1.0049	1.1733	1.0921	1.1555	1.6685	1.4899	1.6815	1.4463	1.4899	1.5968
0.2127	1.0212	1.4317	1.2670	1.3977	2.2437	1.9654	2.2637	1.8960	1.9654	2.1329
0.425	1.0731	1.8280	1.5652	1.7751	3.0254	2.6224	3.0542	2.5213	2.6224	2.8655

Table 4
Energies (in a. u.) of states of the H atom in a uniform magnetic field ($\gamma = 0.0425$, 0.2127 and 0.425) with $n = 1, 2$ are shown. The values listed in column 3 are taken from Table II of Ref. [26]. Eigenvalues of Hamiltonian constructions $\mathbf{H}_1$ (VBR, Def. 3.1) and $\mathbf{H}_2$ (GFBR, Def. 3.2) are included. For each state, the fractional error of the GFBR approximation relative to the VBR result is provided. Quadrature parameters employed for the computation of matrix elements of the local component ${}^{\mathrm{GFBR}}\mathbf{H}_{loc}$ of $\mathbf{H}_2$: $N_r = 6$, ${}^{\mathrm{GFBR}}N_\phi = 15$ and ${}^{\mathrm{GFBR}}N_\theta = 15$.

State	γ	Energies from Ref. [26]	This study		Fractional Error
		Optimized β	Optimized β		Optimized β
			VBR	GFBR	|E(GFBR)−E(VBR)|/E(VBR)
	0.0425	−0.499548	−0.4995	−0.3718	0.2556
$1s$	0.2127	−0.48892	−0.4889	−0.4189	0.1432
	0.425	−0.45802	−0.4581	−0.4018	0.1229
	0.0425	−0.118943	−0.1190	−0.0994	0.1647
$2s$	0.2127	−0.02441	−0.0245	−0.0010	0.9592
	0.425	0.15035	0.1499	0.1828	0.2195
	0.0425	−0.122339	−0.1223	−0.1196	0.0221
$2p_0$	0.2127	−0.07378	−0.0738	−0.0755	0.0230
	0.425	0.02580	0.0255	0.0200	0.2157
	0.0425	-0.09850	−0.0985	−0.0956	0.0294
$2p_1$	0.2127	0.07067	0.0748	0.0752	0.0053
	0.425	0.3352	0.3486	0.3487	0.0003

- GFBR agreement is much worse for the $1s$, $2p_0$ and $2p_{-1}$ states.

It is also instructive to compare columns 4/5 and 6/7 with respect to GFBR accuracy: the quadrature results obtained with the $\{\sigma_{nlm;\beta=1}(r, \theta, \phi)\}$ and $\{\sigma_{nlm;\beta}(r, \theta, \phi)\}$ basis sets are of similar quality only for the $3d_{-1}$ and $3d_{-2}$ states. The $\{\sigma_{nlm;\beta}(r, \theta, \phi)\}$ GFBR performs better for the $1s$, $2p_0$ and $2p_{-1}$ states, whereas the opposite is true for the $2s$ state. The orthonormality of the set $\{\sigma_{nlm;\beta=1}(r, \theta, \phi)\}$ thus does not represent a substantial advantage for the quality of the numerical quadrature as compared to calculations with set $\{\sigma_{nlm;\beta}(r, \theta, \phi)\}$.

Columns 6, 7 and 8 together with Table 1 also prove that the effect of values $\gamma = 0.1$, $\beta \neq 1$ as compared to $\gamma = 0$, $\beta = 1$ on the accuracy of the quadrature rule is not uniform: the $1s$, $2p_0$ and $2p_{-1}$ GFBR energies improve if the magnetic field is applied, whereas the $2s$ energy deteriorates. The reason for this inconsistency is due to the fact that the electronic wave functions are distorted by the magnetic field whereas the quadrature rules for the radial and angular degrees of freedom are only slightly changed and remain invariant, respectively. The aptitude of the resultant quadrature prescription to describe a particular eigenfunction of $\widehat{H}_\gamma(r, \theta, \phi)$ depends mainly on the correspondence between the grid structure and the probability density of the state. The non-orthonormality of the set $\{\chi_{nl;\beta}(r)\}$, and therefore also of the set $\{\sigma_{nlm;\beta}(r, \theta, \phi)\}$ for $\beta \neq 1$, slightly reduces the quadrature precision,

but the effect can be considered insignificant (cf. Sections 4.4.1 and 4.4.2).

The agreement between the energies obtained from the one-basis-function-per-state ansatz with optimized β parameter of Ref. [26] (column 3) and from VBR calculations with the set $\{\sigma_{nlm;\beta}(r, \theta, \phi)\}$ ($\beta \neq 1$) (column 6) is in general good. However, the fact that only one VBR energy is lower than the corresponding entry in column 3 points to some numerical issues in the VBR calculations. The additional variational flexibility introduced by expanding the VBR wave function in the complete set $\{\sigma_{nlm;\beta}(r, \theta, \phi)\}$ (14 functions in total for $n = 1,2,3$) rather than constructing a representation in terms of individual $\sigma_{nlm;\beta}(r, \theta, \phi)$ functions as in Ref. [26] must in principle lead to lower or at best identical energies for any state, independent of the value of β. Tables 2, 4 and 5 show that this is in general not the case, and is due to the fact that some components of the VBR matrix elements could not be evaluated analytically and had to be replaced by numerical approximations (cf. Sections 4.2 and 4.3). The matrix elements of $\widehat{H}_\gamma(r, \theta, \phi)$ provided in Ref. [26], however, have been calculated analytically. The good agreement of energies obtained by the method of Ref. [26] and by our VBR calculations (see Tables 2, 4 and 5) shows that the variational one-basis-function-per-state ansatz is surprisingly accurate. The VBR data suggest that only minor improvements of the energy estimates of Ref. [26] are to be expected if all VBR matrix elements were available analytically.

In Table 4, we report the energies of the $n = 1,2$ states of the H atom in uniform magnetic fields of increasing strength ($\gamma = 0.0425, 0.2127, 0.425$). The β parameters for the $\{\sigma_{nlm;\beta}(r, \theta, \phi)\}$ basis set obtained for $\gamma = 0.0425, 0.2127$ and 0.425 are provided in Table 3.

The results of Table 4 display in general good agreement between the energies calculated in Ref. [26] and the VBR of $\widehat{H}_\gamma(r, \theta, \phi)$ for all values of γ. This is, however, not the case for the GFBR results: the quality of the GFBR predictions for all states depends strongly and very irregularly on the magnetic field. In the case of the $1s/\ 2p_1$ and $2p_0$ states, the quadrature precision improves and deteriorates, respectively, if the magnetic field is intensified. The $2s$ state is particulary interesting as the GFBR estimate fails for $\gamma = 0.2127$ while a higher and similar accuracy is obtained both if γ is reduced as well as amplified. However, the very large fractional error (FE) of 0.9592 obtained for the GFBR energy of the $2s$ state must be considered with this caveat: the FE is commonly a useful gauge for an evaluation of the relative accuracy of computational results but can give a wrong impression if differences between two small numbers are involved as in this case. The deviation of the GFBR from the VBR energy for the $2s$ state is not very large in absolute terms. In order to understand these observations, the effects of the magnetic field strength on the probability densities must be considered. We infer that the low density of the radial lattice is at the core of the problem. An increase of the number of radial grid points should lead to a weaker sensitivity of the GFBR variance to the value of γ and to a generally better match between VBR and GFBR energies.

The GFBR performance for different values of γ is investigated in more detail in Table 5 by also considering lower field strengths and by including $n = 3$ states in addition to $n = 2$ states. We first note a good agreement between energies predicted by the variational approach of Ref. [26] and by the VBR method. Significant relative errors are only obtained for the $\gamma = 0.1$ and $\gamma = 0.2$ calculations of the $3p_{-1}$ state and for the $\gamma = 0.05$ calculation of the $3p_1$ state.

The agreement between VBR and GFBR values is also largely satisfying, but substantial FEs $|\mathrm{E(GFBR)}-\mathrm{E(VBR)}|/\mathrm{E(VBR)}$ are observed for the $2s$, $3s$, $3p_0$ and $3d_0$ states. Again, except for the $2s$ state, these conspicuous FEs are related to differences between small numbers.

6. Conclusions

We have presented a pseudo-spectral approach to the calculation of the electronic motion in atoms or atomic ions with nuclear PE functions or external fields with steep gradients or discontinuities. In particular, we have derived a quadrature rule for the evaluation of matrix elements of local operators between $\sigma_{nlm;\beta}(r, \theta, \phi)$ basis functions. This work builds on the quadrature rule for spherical harmonics $Y_l^m(\theta, \phi)$ presented by Nikiforov et al. [47] in combination with a new quadrature formula for the radial components $\chi_{nl;\beta}(r)$ of eigenstates of H atom-like systems. Nevertheless, the radial quadrature procedure is not linked to any specific angular wave function factor, and it can thus be applied to any eigenfunctions $\chi_{nl;\beta}(r)$ of the radial Hamiltonian (Eq. (4.18)) that are suitable basis functions. However, the use of the sets $\{\chi_{nl;\beta}(r)\}$ and $\{Y_l^m(\theta, \phi)\}$ to assemble product basis functions ensures that the resulting set $\{\sigma_{nlm;\beta}(r, \theta, \phi)\}$ is orthonormal for $\beta = 1$.

It is well known that of the three sets of normalized factors of the H atom eigenfunctions $\{\sigma_{nlm;\beta=1}(r, \theta, \phi)\}$, only the set $\{\nu_m(\phi)\}$ is fully orthonormal, whereas the sets $\{\chi_{nl;\beta=1}(r)\}$ and $\{\zeta_{lm}(\theta)\}$ yield non-diagonal overlap matrices characterized by specific off-diagonal elements of value zero. The linear dependence of the set $\{\zeta_{lm}(\theta)\}$ has been pointed out in Ref [37]. We have here shown that the set $\{\chi_{nl;\beta=1}(r)\}$ is linearly independent and demonstrated that the set $\{\chi_{nl;\beta}(r)\}$ with variationally determined β values according to Ref. [26] can also be transformed into an orthonormal set $\{\widetilde{\chi}_{nl;\beta}(r)\}$, even though Eq. (4.20) does not hold if $\beta \neq 1$. The linear independence of set $\{\chi_{nl;\beta}(r)\}$ for both cases $\beta = 1$ and $\beta \neq 1$ was then used to derive a radial quadrature rule of nearly Gaussian accuracy by adapting the Golub-Welsch scheme [44].

The differentiation between sets $\{\chi_{nl;\beta}(r)\}$ and $\{\zeta_{lm}(\theta)\}$ with respect to orthonormalization has interesting physical implications (Section 4.4.1). Each of the three arrays $\{\chi_{nl;\beta}(r)\}$, $\{\zeta_{lm}(\theta)\}$ and $\{\nu_m(\phi)\}$ may be interpreted as an approximation to a homogeneous set of stationary states of a one-dimensional operator defining electronic motion. The only orthonormal set of basis functions is $\{\nu_m(\phi)\}$ and this set is related to, but not identical with, the homogeneous set of eigenfunctions of a single, parameter-independent operator (cf. Section 4.4.1).

Both $\{\chi_{nl;\beta=1}(r)\}$ and $\{\zeta_{lm}(\theta)\}$ were shown to be non-orthonormal and inhomogeneous sets of eigenstates because of their l- and m-dependence, respectively. The complete sets $\{\chi_{nl;\beta=1}(r)\}$ and $\{\zeta_{lm}(\theta)\}$ therefore do not span eigenspaces of parameter-independent Hermitian operators and the elements included in both sets, although they are eigenfunctions, do not describe uncoupled electronic motion as is the case for the elements of the set $\{\nu_m(\phi)\}$. We have shown that the different conditions for orthonormalization distinguish the set $\{\chi_{nl;\beta=1}(r)\}$ from the set $\{\zeta_{lm}(\theta)\}$. The coupling of the set $\{\zeta_{lm}(\theta)\}$ to the set $\{\nu_m(\phi)\}$ is essential in order to obtain an orthonormal homogeneous set of eigenfunctions of the $\hat{L}^2(\theta, \phi)$ operator, i.e., the set $\{Y_l^m(\theta, \phi)\}$. In a similar manner, the elements of the set $\{\widetilde{\chi}_{nl;\beta=1}(r)\}$ do not span an eigenspace, but the fact that the overlap matrix is diagonal allows us to interpret the $\widetilde{\chi}_{nl;\beta=1}(r)$ functions as approximations to eigenstates of a common parameter-independent operator.

We can therefore establish a ranking of these sets with respect to their degree of representation of one-dimensional electronic orbitals: the elements of the set $\{\nu_m(\phi)\}$ are orthonormal and can be viewed as contained (because of the definition interval $[0, 2\pi]$) stationary states. The array $\{\chi_{nl;\beta=1}(r)\}$ can be linearly transformed into the orthonormal set $\{\widetilde{\chi}_{nl;\beta=1}(r)\}$ which mimics a homogeneous set of eigenfunctions. The items of the set $\{\zeta_{lm}(\theta)\}$ must be linked to elements of the set $\{\nu_m(\phi)\}$ in order to form two-dimensional eigenstates $Y_l^m(\theta, \phi)$. The radial components $\chi_{nl;\beta=1}(r)$ of H atom eigenfunctions $\sigma_{nlm;\beta=1}(r, \theta, \phi)$ thus have a higher level of separability from the spherical harmonics compared to the strong coupling between the $\zeta_{lm}(\theta)$ and $\nu_m(\phi)$ factors.

The quadrature rules derived were applied to two model systems, the field-free H atom and the H atom in a uniform magnetic field model. The variational one-basis-set-per-state ansatz presented in Ref. [26] was used to define the basis functions and for providing comparative data.

We found very good agreement between the energies of Ref. [26] and the energies obtained using the VBR, demonstrating that the additional variational flexibility provided by the VBR calculation is insignificant for this particular basis set and model system. In contrast, large differences between VBR energies and their GFBR counterparts

Table 5
Energies (in Rydberg units ($=\frac{1}{2}$ a. u.)) of states of the H atom in a uniform magnetic field (γ = 0.005, 0.02, 0.05, 0.1 and 0.2) with n = 2, 3 are shown. The values listed for each state in the first, second and third line are taken from Table III of Ref. [26], are eigenvalues of $\mathbf{H}_1$ (VBR, Def. 3.1) and are eigenvalues of $\mathbf{H}_2$ (GFBR, Def. 3.2), respectively. Quadrature parameters employed for the computation of matrix elements of the local component ${}^{\mathrm{GFBR}}\mathbf{H}_{loc}$ of $\mathbf{H}_2$: $N_r = 6$, ${}^{\mathrm{GFBR}}N_\phi = 15$ and ${}^{\mathrm{GFBR}}N_\theta = 15$.

State	$\gamma = 0.005$	0.02	0.05	0.1	0.2
$2s$	−0.2498	−0.2472	−0.2335	−0.1916	−0.06715
	−0.2498	−0.2472	−0.2335	−0.1916	−0.0672
	−0.2019	−0.2070	−0.1939	−0.1497	−0.0216
$2p_{-1}$	−0.2548	−0.2676	−0.2857	−0.2990	−0.2879
	−0.2549	−0.2676	−0.2856	−0.2976	−0.2804
	−0.2424	−0.2602	−0.2800	−0.2940	−0.2795
$2p_0$	−0.2499	−0.2488	−0.2427	−0.2227	−0.1575
	−0.2499	−0.2488	−0.2427	−0.2227	−0.1576
	−0.2375	−0.2414	−0.2374	−0.2202	−0.1623
$2p_1$	−0.2448	−0.2276	−0.1857	−0.0990	0.1120
	−0.2449	−0.2276	−0.1856	−0.0976	0.1196
	−0.2324	−0.2202	−0.1800	−0.0940	0.1205
$3s$	−0.1102	−0.09860	−0.05025	0.06247	0.3339
	−0.1103	−0.0986	−0.0503	0.0625	0.3340
	−0.0907	−0.0832	−0.0284	0.0960	0.3821
$3p_{-1}$	−0.1152	−0.1181	−0.09814	−0.03218	0.1464
	−0.1152	−0.1178	−0.0954	−0.0223	0.1739
	−0.1065	−0.1149	−0.0936	−0.0211	0.1736
$3p_0$	−0.1106	−0.1043	−0.0755	−0.0033	0.1782
	−0.1107	−0.1043	−0.0755	−0.0034	0.1782
	−0.1019	−0.1016	−0.0753	−0.0058	0.1637
$3p_1$	−0.1052	−0.07810	0.00186	0.1678	0.5464
	−0.1052	−0.0778	0.0046	0.1777	0.5739
	−0.0965	−0.0749	0.0064	0.1789	0.5736
$3d_{-2}$	−0.1204	−0.1411	−0.1612	−0.1656	−0.1318
	−0.1204	−0.1410	−0.1597	−0.1599	−0.1155
	−0.1116	−0.1378	−0.1576	−0.1583	−0.1157
$3d_{-1}$	−0.1156	−0.1243	−0.1255	−0.1033	−0.02176
	−0.1157	−0.1243	−0.1254	−0.1029	−0.0205
	−0.1068	−0.1210	−0.1231	−0.1007	−0.0186
$3d_0$	−0.1107	−0.1053	−0.08063	−0.01727	0.1444
	−0.1107	−0.1054	−0.0806	−0.0173	0.1445
	−0.1019	−0.1025	−0.0806	−0.0209	0.1242
$3d_1$	−0.1056	−0.08431	−0.02550	0.09664	0.3782
	−0.1057	−0.0843	−0.0254	0.0971	0.3795
	−0.0968	−0.0810	−0.0231	0.0993	0.3814
$3d_2$	−0.1004	−0.06114	0.03879	0.2343	0.6681
	−0.1004	−0.0610	0.0403	0.2401	0.6845
	−0.0916	−0.0578	0.0424	0.2417	0.6843

were in many cases observed. Our analysis demonstrated that the low GFBR accuracy obtained for the 1s state could be related to an insufficient density of the radial lattice $\{r_k\}$.

We also found that there is a complex, and non-systematic, dependence of the error on γ for the GFBR energy of an individual state. However, we showed that the more inaccurate GFBR energies of the 2s and 3s states as compared to the 2p, 3p and 3d results could be traced to the fact that, for a common n, the radial probability densities of $l = 0$ states have one and two nodes more than $l = 1$ and $l = 2$ densities, respectively.

If the condition of orthonormality of the basis set in the VBR would be the main criterion for a minimal variance of GFBR energy estimates from VBR reference values, then the $\gamma = 0$, $\beta = 1$ GFBR results should in general be more accurate than the corresponding energies calculated for $\gamma \neq 0$, $\beta \neq 1$. However, we found that the accuracy of the GFBR energies for different values of γ varies in a nonuniform manner, and thus that other factors, such as the correspondence between grid structure and probability density distribution, are more important for the quality of the quadrature approximation in form of the matrix ${}^{\mathrm{GFBR}}\mathbf{H}_{loc}$ to ${}^{\mathrm{VBR}}\mathbf{H}_{loc}$.

Finally we discuss the potential of the VBR and GFBR methods for the accurate description of electronic states in atoms and atomic ions. Ref. [26] considers only small to moderate field intensities up to γ = 0.425 and we have adopted this limit in the calculations performed for the present study. It would be interesting to investigate to which magnitude of γ an ansatz relying exclusively on $\sigma_{nlm;\beta}(r, \theta, \phi)$ basis functions yields quantitative accuracy for eigenstates of the H atom in a uniform magnetic field.

We have not explored the application range available with the basis set $\{\sigma_{nlm;\beta}(r, \theta, \phi)\}$. However, it is clear that basis functions derived from the spherical field-free H atom-like model are not appropriate for the description of eigenfunctions in a magnetic field regime significantly exceeding the Coulomb limit ($\gamma \to 0$). This restriction is due to the gradual transition of the symmetry of the system from spherical to cylindrical as the magnetic field strength increases towards the Landau limit ($\gamma \to \infty$) [55,56].

For example, Ref. [56] suggests an approach formulated in terms of a parabolic coordinate system and featuring basis functions distinguished by three variational parameters that allows for an adiabatic interchange from Coulomb to Landau basis sets as the value of γ is growing.

Because the Hamiltonian constructions $\mathbf{H}_1$ (VBR, Def. 3.1) and $\mathbf{H}_2$ (GFBR, Def. 3.2) correspond to exact and approximate representations in terms of the $\{\sigma_{nlm;\beta}(r, \theta, \phi)\}$ basis set, respectively, they are not appropriate for the description of the H atom in strong external electromagnetic fields which induce a substantial deformation of the eigenfunctions away from the spherical symmetry of the field-free system. This restriction applies generally to VBR and GFBR calculations on atoms or atomic ions if the eigenstates are expanded only in terms of the $\{\sigma_{nlm;\beta}(r, \theta, \phi)\}$ basis set. Both the VBR and GFBR approaches outlined in this work should, however, be suitable for the treatment of multi-electron atoms and atomic ions in weak to moderate electromagnetic fields.

The accuracy of the GFBR approximations compiled in Tables 1, 2, 4 and 5 is certainly far from quantitative. The presentation of GFBR results that are not fully converged with respect to N_r, ${}^{\mathrm{GFBR}}N_\theta$ and ${}^{\mathrm{GFBR}}N_\phi$ in the four tables should also be seen in the context of the primarily method-oriented nature of this study. High-precision GFBR calculations will be performed for subsequent projects.

We are convinced that convergence with respect to the size of the full quadrature grid can be reached and that the GFBR method can then provide quantitative accuracy for systems significantly more complex than the two models considered in the present study.

The flexibility of the quadrature rule for the spherical harmonics discussed in Section 4.4.3 allows for the choice of arbitrary grid sizes for the θ and ϕ degrees of freedom.

However, the application of the procedure defined in Section 4.4.2 to the computation of radial grids $\{r_k\}$ of increasing size as described in Section 5.1 (cf. Fig. 1) has shown that construction of the orthonormal set $\{\tilde{\chi}_{nl;\beta}(r)\}$ with Löwdin symmetric orthogonalization, and therefore the evaluation of $\{r_k\}$, becomes numerically progressively difficult with increasing n_{max}.

We are planning to investigate methods that can be alternatives to the Gram-Schmidt or Löwdin orthogonalization schemes for the resolution of linear independence for $n_{max} > 5$. One option is to select subsets of the set $\{\chi_{nl;\beta}(r)\}$ for larger values of n_{max} that can be orthonormalized by employing the Gram-Schmidt or Löwdin procedures. This ansatz would yield reduced lattices $\{r_k\}$ with a smaller number of grid points as compared to the dimension of the radial basis set $\{\chi_{nl;\beta}(r)\}$.

If implemented, this approach may permit the specification of 'reduced' radial lattices for large values of n_{max}. The GFBR approach

should then, e.g., allow for the modelling of highly charged ions with high-Z nuclei (with Z denoting the number of protons), taking relativistic, finite nuclear size and quantum electrodynamics (QED) corrections into account in the framework of a wave function ansatz. The accurate computation of molecular Rydberg states, e.g. of benzene, represents another possible application of the GFBR method.

We expect that the GFBR method has the potential to provide a more convenient realization and a significantly better computational efficiency of programs developed for the simulation of these challenging systems than implementations based on global spectral techniques.

Acknowledgments

C.W. would like to thank the Tromsø Research Foundation (through funds by Trond Mohn, Grant Nr. A32542) and W. Domcke for support. This work has received funding from the Research Council of Norway through a Centre of Excellence grant (Grant Nr. 177558). We also acknowledge grants for computer time provided by the Norwegian High Performance Computing (NOTUR, Grant Nr. NN4654K) and the Leibniz Supercomputing Centre in München.

Appendix A. Grid-based vs. spectral approaches in electronic-structure theory

In this appendix, we will discuss some of the differences between grid-based and global spectral approaches in the numerical solution of the TDSE, TISE and Density Functional Theory (DFT) equations.

As mentioned under item (i) in Section 1, the challenges global spectral methods have in describing solutions featuring sharp gradients or discontinuities can also affect quantum-chemical calculations even in the absence of external fields, e.g., due to the "Coulomb singularity" or "Kato cusp condition" [57,20,58,3,4]. However, the negative effect of the Coulomb singularity on the convergence properties of global spectral methods is usually not relevant in practical applications since most applications do not focus on the computation of the absolute energies of electronic states. Furthermore, there is seldom a need for a very accurate description of the motion of electrons in the vicinity of the nuclei, as chemistry is largely determined by the valence electrons, and this explains the popularity of approximations such as Effective Core Potentials (ECPs) [59–62].

Except for the Coulomb singularity problem, spectral methods are well suited for the computation of the electronic motion in smooth Coulomb-type potentials because the reduced accuracy of basis-set representations for problems that include solutions characterized by sharp gradients or discontinuities can be avoided. However, this is no longer the case if a precise description of the electronic motion in strong internal or external fields is required. With the advent of fourth-generation light sources, such problems are of increasing experimental and theoretical interest [63], and computational methods capable of accurately describing the physics in these situations are needed.

Let us first consider the case of strong internal fields. As long as the Coulomb singularity aspect can be neglected and no heavy elements are involved, the inner electrons are to a good approximation experiencing Coulomb-type potentials and can be well described in terms of GTOs [64] or STOs. However, the simple picture of electrons moving in nuclear Coulomb fields becomes inappropriate if strong electromagnetic interactions need to be accounted for. An accurate representation of the electronic motion in strong nuclear fields requires that also the effects of the finite nuclear size as well as relativistic and QED corrections are accounted for [65–70].

For lighter nuclei, electronic-structure calculations of highly charged ions have been performed by employing spectral methods in a non-relativistic approach [71]. Spectral methods have also been used for calculating strong-field [72,73] and relativistic effects [74–78].

For low-Z nuclei, the nucleus-electron interaction can in a QED framework be expanded in the parameter $(Z\alpha)$, with α denoting the fine-structure constant. However, for high-Z systems, an approach which is non-perturbative in $(Z\alpha)$ is required [79]. Spectral methods for computing QED corrections of high-Z systems have been developed [79], but the complex geometries and discontinuous coefficients characteristic of electronic orbitals in strong nuclear fields make the design of grid-based concepts attractive [80,81].

The same arguments, in this case independent of Z, hold for the description of atoms and molecules in time-independent and time-dependent strong electromagnetic fields. In atoms, strong external fields may destroy the spherical symmetry of the nuclear Coulomb potentials and, due to the superposition of internal and external fields, can induce PE functions of complex topology. Nuclear Coulomb-type potentials are similarly prevailing, at smaller radii, in molecules, and strong external fields may disturb these nearly centrosymmetric fields determining the motion of core electrons also in polyatomic systems.

For lighter nuclei, spectral methods have been applied to the treatment of electronic motion in such combined stationary [82–84,17,85,15,86] and fluctuating [87,14] electromagnetic fields. Real-space lattice representations are nevertheless an interesting alternative approach, and such studies have been reported for the H and He atoms, for the H_2^+ and H^- ions as well as for the H_2 molecule in strong time-independent [16,88–92,57,20] and time-dependent [93–96] electromagnetic fields.

Item (ii) quoted in Section 1 will be discussed next. Whereas global spectral methods are dominating electronic structure calculations on non-periodic systems using atom-centered GTO and STO basis sets, they are also being used in calculations on periodic systems, with plane-wave basis sets being the standard choice [97–100,6,101]. Like grid-based methods, plane-wave basis sets have the advantage that the linear dependence problem can be avoided due to the orthogonality of the basis functions and that no BSSE can arise because of the definition of a global computational cell which includes the reaction partners.

However, there are also drawbacks to plane-wave basis sets [6]. Real-space grid techniques that for instance allow Wannier functions to be represented [102] are therefore playing a more important role in the treatment of periodic systems [103] compared to non-periodic ensembles. The advantages of grid-based methods over plane-wave basis sets are summarized in Ref. [104].

The relevance of a grid-based approach to the description of periodic systems is also obvious from the correspondence between delocalized plane-wave functions and equidistantly spaced support meshes which forms the foundation of the Fast Fourier Transform (FFT) method for the evaluation of the kinetic energy operator in wave function propagation schemes [105].

Real-space lattice methods are not only developed for dealing with the extreme scenarios described under item (i) in Section 1 or as an alternative to plane-wave basis sets for periodic systems. They are also utilized as an alternative to GTOs and STOs for computations of electronic states of atoms, molecules and non-periodic materials. Refs. [106,107] provide an overview of relevant applications of DFT and of wave function formalisms. The value of a representation of the electronic wave function on a support mesh for a description of model systems like the H and He atoms as well as of the H_2^+ ion is demonstrated in Refs. [108–112,96,113]. Refs. [104,114–116] report grid-based concepts for the modelling of mainly non-periodic systems in a non-relativistic DFT framework.

Finite element methods (FEMs) have been developed for the non-relativistic and relativistic calculation of atomic [117–120] and molecular [121–124,5,125,120,126] wave functions. Another application of FEMs are non-relativistic [127–129] and relativistic DFT calculations [130,131] of molecules. The role of FEMs for DFT-based simulations of solids have been discussed by Pask et al. [132–134], Gavini et al. [135] and Masud et al. [4].

Finally, we address item (iii) of Section 1, the convenient mapping of local operators in grid-based numerical schemes for the solution of the TDSE and TISE. If analytical expressions of local operators are

available, then global spectral methods usually allow for a straightforward construction of the corresponding matrix representations. However, quantum–mechanical problems are frequently characterized by an original definition of local operators on real-space grids and analytical formulae may only be derived via elaborate fitting procedures. In nuclear quantum dynamics, e.g., discrete approximations of PE surfaces are in general obtained by performing electronic structure calculations at appropriate molecular geometries. Grid-based methods for the solution of the TDSE and TISE allow for a direct integration of the resulting PE matrices in the Hamiltonian operators describing the nuclear motion, bypassing the need to develop an analytical form of the PE surfaces. The direct use of local operator matrix elements defined on grid points explains the popularity of the FFT [105] and DVR [28,1,29,30] schemes for the quantum–mechanical treatment of nuclear motion.

As noted under item (i) in Section 1, grid-based techniques are of relevance for the description of electronic motion in strong internal and external fields because they may provide higher accuracy than global spectral methods in these cases. The Gibbs phenomenon, though, is not the only motivation for grid representations if electrons are to be modelled in strong-field environments. Local field operators may not be available in analytical form from the outset, being instead defined on a real-space mesh. This, in combination with the robustness of real-space grid-based methods for ill-behaved functions, suggests that a representation of local operators on a support lattice may yield both a more accurate and a more convenient picture of electronic orbitals in strong fields.

References

[1] J.C. Light, T. Carrington Jr., Discrete-variable representations and their utilization, in: I. Prigogine, S.A. Rice (Eds.), Advances in Chemical Physics, 114 John Wiley & Sons Inc, New York, 2007, pp. 263–310, , https://doi.org/10.1002/9780470141731.ch4.
[2] S. Abarbanel, D. Gottlieb, E. Tadmor, Spectral methods for discontinuous problems, in: K.W. Morton, M.J. Baines (Eds.), Numerical Methods for Fluid Dynamics, II Oxford University Press, 1986, pp. 128–153.
[3] T.J.R. Hughes, J.A. Cottrell, Y. Bazilevs, Comput. Methods Appl. Mech. Eng. 194 (2005) 4135–4195.
[4] A. Masud, A. Al-Naseem, R. Kannan, H. Gajendran, J. Appl. Mech. 85 (2018) 091009.
[5] C. Düsterhöft, D. Heinemann, D. Kolb, Chem. Phys. Lett. 296 (1998) 77–83.
[6] G.H. Booth, T. Tsatsoulis, G.K.-L. Chan, A. Grüneis, J. Chem. Phys. 145 (2016) 084111.
[7] B. Klahn, Adv. Quantum Chem. 13 (1981) 155–209.
[8] S. Wilson, Many-body perturbation theory and its application to the molecular electronic structure problem, in: A. Hinchliffe (Ed.), Chemical Modelling: Applications and Theory, Vol. 1 Royal Society of Chemistry, London, 2000, pp. 364–452.
[9] I.G. Kaplan, Intermolecular Interactions: Physical Picture, Computational Methods and Model Potentials, John Wiley & Sons, 2006.
[10] I. Mayer, Theor. Chim. Acta 72 (1987) 207–210.
[11] A. Hamza, A. Vibok, G.J. Halasz, I. Mayer, J. Mol. Struct. 501–502 (2000) 427–434.
[12] K. Lee, J. Yu, Y. Morikawa, Phys. Rev. B 75 (2007) 045402.
[13] Y.P. Kravchenko, M.A. Liberman, B. Johansson, Phys. Rev. A 54 (1996) 287–305, https://doi.org/10.1103/PhysRevA.54.287.
[14] D. Delande, K.T. Taylor, M.H. Halley, T. van der Veldt, W. Vassen, W. Hogervorst, J. Phys. B: At. Mol. Opt. Phys. 27 (13) (1994) 2771 URL http://stacks.iop.org/0953-4075/27/i=13/a=008.
[15] J. Xi, X. He, B. Li, Phys. Rev. A 46 (1992) 5806–5811, https://doi.org/10.1103/PhysRevA.46.5806.
[16] W. Schweizer, P. Faßbinder, R. González-Ferez, M. Braun, S. Kulla, M. Stehle, J. Comput. Appl. Math. 109 (1999) 95–122.
[17] A.V. Turbiner, J.C. López, Vieyra, Phys. Rep. 424 (2006) 309–396.
[18] A.V. Turbiner, J. Phys. A: Math. Gen. 17 (1984) 859–875.
[19] H. Friedrich, D. Wintgen, Phys. Rep. 183 (2) (1989) 7–79 URL http://www.sciencedirect.com/science/article/pii/037015738990121X.
[20] Z. Sun ArXiv:1604.00731v1 [physics.comp-ph].
[21] A. Poszwa, A. Rutkowski, Phys. Rev. A 63 (2001) 043418.
[22] Y.P. Kravchenko, M.A. Liberman, B. Johansson, Phys. Rev. Lett. 77 (1996) 619–622.
[23] Y.P. Kravchenko, M.A. Liberman, Int. J. Quant. Chem. 62 (1997) 593–601.
[24] A. Rutkowski, A. Poszwa, Phys. Rev. A 67 (2003) 013412.
[25] J.A.C. Gallas, E. Gerck, R.F. O'Connell, Phys. Rev. Lett. 50 (1983) 324–327.
[26] J.A.C. Gallas, Phys. Rev. A 29 (1984) 132–136.
[27] G. Czakó, V. Szalay, A.G. Császár, J. Chem. Phys. 124 (2006) 014110.
[28] J.C. Light, I.P. Hamilton, J.V. Lill, J. Chem. Phys. 82 (1985) 1400.
[29] C. Woywod, Chem. Phys. Lett. 281 (1997) 168.
[30] C. Woywod, Mol. Phys. 95 (1998) 713.
[31] D.G. McGavin, W.C. Tennant, J. Magn. Reson. 87 (1990) 92–109.
[32] D.O. Harris, G.G. Engerholm, W.D. Gwinn, J. Chem. Phys. 43 (1965) 1515.
[33] A.S. Dickinson, P.R. Certain, J. Chem. Phys. 49 (1968) 4209.
[34] MATLAB version 7.11.0, The MathWorks Inc., Natick, Ma, USA, 2010.
[35] L.F. Shampine, J. Comput. Appl. Math. 211 (2) (2008) 131–140.
[36] C. Hwang, S.-K. Chen, Geophys. J. Int. 129 (1997) 450–460.
[37] X.-G. Wang, T. Carrington Jr, Mol. Phys. 110 (2012) 825–835.
[38] R. Zippel, in: Effective Polynomial Computation, The Springer International Series in Engineering and Computer Science Vol. 241 Springer, US, New York, 1993.
[39] M. Zworski, Semiclassical Analysis, Graduate Studies in Mathematics Vol. 138 American Mathematical Society, Providence, Rhode Island, 2012.
[40] P.-O. Löwdin, J. Chem. Phys. 18 (1950) 365.
[41] I. Mayer, Int. J. Quant. Chem. 90 (2002) 63–65.
[42] D.T. Colbert, W.H. Miller, J. Chem. Phys. 96 (1992) 1982.
[43] G.C. Groenenboom, D.T. Colbert, J. Chem. Phys. 99 (1993) 9681.
[44] G.H. Golub, J.H. Welsch, Math. Comp. 23 (1969) 221–230.
[45] G.C. Corey, D. Lemoine, J. Chem. Phys. 97 (6) (1992) 4115–4126 URL http://scitation.aip.org/content/aip/journal/jcp/97/6/10.1063/1.463916.
[46] L. Lodi, J. Tennyson, J. Phys. B: At. Mol. Opt. Phys. 43 (2010) 133001.
[47] A.F. Nikiforov, S.K. Suslov, V.B. Uvarov, C.A.J. Fletcher, R. Glowinski, W. Hillebrandt, M. Holt, P. Hut, H.B. Keller, J. Killeen, S.A. Orszag, V.V. Rusanov (Eds.), Classical Orthogonal Polynomials of a Discrete Variable, Springer Series in Computational Physics, Springer-Verlag, 1991.
[48] D. Caballero, Discrete variable representation of the angular variables in quantum three-body scattering, Ph.D. thesis School of Mathematical Sciences, Claremont Graduate University, 2011.
[49] K.H. Kwon, L.L. Littlejohn, J. Korean Math. Soc. 34 (1997) 973–1008.
[50] Y.L. Luke (Ed.), The special functions and their approximations: Vol. 53-I of Mathematics in Science and EngineeringAcademic Press, New York, 1969, pp. 1–349.
[51] F. Brafman, Quart. J. Math. Oxford 10 (1959) 156–160.
[52] D. de Fazio, S. Cavalli, V. Aquilanti, Int. J. Quant. Chem. 93 (2003) 91–111.
[53] E. Diekema, Mathematics 3 (2015) 487–509.
[54] A. Ries, Prog. Phys. 3 (2012) 29.
[55] S.P. Goldman, M.M. Cassar, Atoms in strong fields, in: G.W.F. Drake (Ed.), Springer Handbook of Atomic, Molecular, and Optical Physics, Springer Handbooks, Springer, New York, 2006, pp. 227–234.
[56] J.A.C. Gallas, J. Phys. B: At. Mol. Opt. Phys. 18 (1985) 2199–2206.
[57] J. Shen, Y. Wang, H. Yu, Efficient spectral-element methods for the electronic schrödinger equation, in: J. Garcke, D. Pflüger (Eds.), Sparse Grids and Applications – Stuttgart 2014, Lecture Notes in Computational Science and Engineering, Vol. 109 Springer International Publishing, Cham, 2016, pp. 265–289.
[58] J.R. Jones, F.-H. Rouet, K.V. Lawler, E. Vecharynski, K.Z. Ibrahim, S. Williams, B. Abeln, C. Yang, W. McCurdy, D.J. Haxton, X.S. Li, T.N. Rescigno, Mol. Phys. 114 (2016) 2014–2028.
[59] M. Dolg, Effective core potentials, in: J. Grotendorst (Ed.), Modern Methods and Algorithms of Quantum Chemistry, NIC series, Vol. 1 John von Neumann Institute for Computing, Jülich, 2000, pp. 479–508.
[60] M. Dolg, Lanthanides and actinides, in: P. Schleyer, et al. (Ed.), Encyclopedia of Computational Chemistry, Vol. 2 Wiley and Sons, Chichester, 1998, p. 1478.
[61] M. Dolg, H. Stoll, Electronic structure calculations for molecules containing lanthanide atoms, in: K.A. Gschneider, L. Eyring (Eds.), Handbook on the Physics and Chemistry of the Rare Earths, 22 Elsevier, 1996, p. 607.
[62] A. Bergner, M. Dolg, W. Kuechle, H. Stoll, H. Preuss, Mol. Phys. 80 (1993) 1431.
[63] M.E. Couprie, J. Electron Spectrosc. Relat. Phenom. 196 (2014) 3–13.
[64] J.L. Jerke, Y. Lee, C.J. Tymczak, J. Chem. Phys. 143 (2015) 064108.
[65] A. Pálffy, Contemp. Phys. 51 (2010) 471–496.
[66] U.D. Jentschura, Phys. Rev. A 92 (2015) 012123.
[67] V.P. Neznamov, I.I. Safronov, Phys. Usp. 57 (2014) 189–193.
[68] V.M. Shabaev, J. Phys. B, At. Mol. Opt. Phys. 26 (1993) 1103.
[69] B.N. Niri ArXiv:1612.08042v1 [physics.atom-ph].
[70] B. Nickel, J. Phys. B, At. Mol. Opt. Phys. 46 (2013) 015001.
[71] G. Friesecke, B.D. Goddard, Phys. Rev. A 81 (2010) 032516.
[72] A.Y. Potekhin, G.G. Pavlov, Astrophys. J. 407 (1993) 330–341.
[73] W. Zhu, S.B. Trickey ArXiv:1709.05553v1 [physics.comp-ph].
[74] S.R. McConnell, A.N. Artemyev, M. Mai, A. Surzhykov, Phys. Rev. A 86 (2012) 052705.
[75] A. Surzhykov, J.P. Santos, P. Amaro, P. Indelicato, Phys. Rev. A 80 (2009) 052511.
[76] G. Singh, N.K. Puri, J. Phys. B, At. Mol. Opt. Phys. 49 (2016) 205002.
[77] T. Bastug, W.-D. Sepp, D. Kolb, B. Fricke, E.J. Baerends, G. Te Velde, J. Phys. B: At. Mol. Opt. Phys. 28 (1995) 2325–2331.
[78] C.J. Fontes, H.L. Zhang, J. Abdallah Jr, R.E.H. Clark, D.P. Kilcrease, J. Colgan, R.T. Cunningham, P. Hakel, N.H. Magee, M.E. Sherrill, J. Phys. B: At. Mol. Opt. Phys. 48 (2015) 144014.
[79] H. Persson, S. Salomonson, P. Sunnergren, I. Lindgren, M.G.H. Gustavsson, Hyp. Int. 108 (1997) 3–17.
[80] A.I. Bondarev, Y.S. Kozhedub, N.S. Oreshkina, Opt. Spectrosc. 109 (2010) 823–828.
[81] D.H. Sampson, H.L. Zhang, C.J. Fontes, Phys. Rep. 477 (2009) 111–214.
[82] P. Krause, J.A. Sonk, H.B. Schlegel, J. Chem. Phys. 140 (2014) 174113.
[83] J.-J. Zhao, X.-F. Wang, H.-X. Qiao, Chin. Phys. B 20 (2011) 053101.

[84] R.A. Lewis, A. Bruno-Alfonso, G.V.B. de Souza, R.E.M. Vickers, J.A. Colla, E. Constable, Sci. Rep. 3 (2013) 3488.
[85] C.W. McCurdy, T.N. Rescigno, Phys. Rev. A 35 (1987) 657–663.
[86] Y. Zhang, Q. Liu, T. Shi, J. Phys. B: At. Mol. Opt. Phys. 45 (8) (2012) 085101 URL http://stacks.iop.org/0953-4075/45/i=8/a=085101.
[87] K. Varga, Phys. Rev. E 85 (2012) 016705, https://doi.org/10.1103/PhysRevE.85.016705.
[88] P. Fassbinder, W. Schweizer, Phys. Rev. A 53 (1996) 2135.
[89] T.N. Rescigno, D.A. Horner, F.L. Yip, C.W. McCurdy, Phys. Rev. A 72 (2005) 052709 URL http://link.aps.org/doi/10.1103/PhysRevA.72.052709.
[90] G.P. Sasmal, J. At. Mol. Sci. 5 (2014) 187–205.
[91] J. Shertzer, L.R. Ram-Mohan, D. Dossa, Phys. Rev. A 40 (1989) 4777–4780.
[92] Y.P. Kravchenko, M.A. Liberman, Phys. Rev. A 56 (1997) R2510–R2513.
[93] L.-Y. Peng, A.F. Starace, J. Chem. Phys. 125 (2006) 154311.
[94] A. Picón, A. Jaroń-Becker, A. Becker, Phys. Rev. Lett. 109 (2012) 163002.
[95] X.-M. Tong, S.-I. Chu, Chem. Phys. 217 (1997) 119–130.
[96] G.-Z. Kiss, S. Borbély, L. Nagy, AIP Conf. Proc. 1694 (2015) 020017.
[97] J.J. Shepherd, A. Grüneis, G.H. Booth, G. Kresse, A. Alavi, Phys. Rev. B 86 (2012) 1–14.
[98] J.J. Shepherd, G.H. Booth, A. Alavi, J. Chem. Phys. 136 (2012) 244101.
[99] A. Grüneis, J.J. Shepherd, A. Alavi, D.P. Tew, G.H. Booth, J. Chem. Phys. 139 (2013) 084112.
[100] J.J. Shepherd, A. Grüneis, Phys. Rev. Lett. 110 (2013) 1–5.
[101] M. Marsman, A. Grüneis, J. Painer, G. Kresse, J. Chem. Phys. 130 (2009) 184103.
[102] A.A. Mostofi, C.-K. Skylaris, P.D. Haynes, M.C. Payne, Comp. Phys. Comm. 147 (2002) 788–802.
[103] A. Natan, A. Benjamini, D. Naveh, L. Kronik, M.L. Tiago, S.P. Beckman, J.R. Chelikowsky, Phys. Rev. B 78 (2008) 075109.
[104] J.-L. Fattebert, M.B. Nardelli, Finite difference methods for ab initio electronic structure and quantum transport calculations of nanostructures, in: P.G. Ciarlet, C. Le Bris (guest editor) (Eds.), Special Volume Computational Chemistry, Vol. X of Handbook of Numerical Analysis, Elsevier Science B.V., Amsterdam, 2003, pp. 571–612.
[105] D. Kosloff, R.A. Kosloff, J. Comput. Phys. 52 (1983) 35.
[106] Y. Saad, J.R. Chelikowsky, S.M. Shontz, SIAM Rev. 52 (2010) 3–54.
[107] L. Frediani, D. Sundholm, Phys. Chem. Chem. Phys. 17 (2015) 31357.
[108] H.-J. Flad, W. Hackbusch, D. Kolb, R. Schneider, J. Chem. Phys. 116 (2002) 9641.
[109] H.-J. Flad, W. Hackbusch, H. Luo, D. Kolb, J. Comput. Phys. 205 (2005) 540–566.
[110] J. Ackermann, Phys. Rev. A 52 (1995) 1968.
[111] J. Ackermann, J. Shertzer, Phys. Rev. A 54 (1996) 365–371.
[112] J. Ackermann, Phys. Rev. A 57 (1998) 4201–4203.
[113] D.-Q. Yu, S.-L. Cong, D.H. Zhang, Z.-G. Sun, Chin. J. Chem. Phys. 26 (2013) 755–764.
[114] J.R. Chelikowsky, Y. Saad, S. Ögüt, I. Vasiliev, A. Stathopoulos, Phys. Stat. Sol. (b) 217 (2000) 173–195.
[115] X. Andrade, D. Strubbe, U. De Giovannini, A.H. Larsen, M.J.T. Oliveira, J. Alberdi-Rodriguez, A. Varas, I. Theophilou, N. Helbig, M.J. Verstraete, L. Stella, F. Nogueira, A. Aspuru-Guzik, A. Castro, M.A.L. Marques, A. Rubio, Phys. Chem. Chem. Phys. 17 (2015) 31371–31396.
[116] T.L. Beck, Rev. Mod. Phys. 72 (2000) 1041–1080.
[117] D. Sundholm, J. Olsen, P.Å. Malmquist, B.O. Roos, M. Defranceschi, J. Delhalle (Eds.), NATO advanced research workshop, Versaille, 1988, Vol. 271 of NATO ASI series C, 1989, p. 329.
[118] D. Sundholm, J. Olsen, J. Chem. Phys. 94 (1991) 5051.
[119] H. Almanasreh, S. Salomonson, N. Svanstedt, J. Comput. Phys. 236 (2013) 426–442.
[120] S.R. White, J.W. Wilkins, M.P. Teter, Phys. Rev. B 39 (1989) 5819–5833.
[121] W. Schulze, D. Kolb, Chem. Phys. Lett. 122 (1985) 271.
[122] D. Heinemann, B. Fricke, D. Kolb, Phys. Rev. A 38 (1988) 4994.
[123] L. Yang, D. Heinemann, D. Kolb, Chem. Phys. Lett. 192 (1992) 499.
[124] L. Yang, D. Heinemann, D. Kolb, Phys. Rev. A 48 (1993) 2700.
[125] C. Düsterhöft, L. Yang, D. Heinemann, D. Kolb, Chem. Phys. Lett. 229 (1994) 667.
[126] J. Ackermann, R. Roitzsch, Chem. Phys. Lett. 214 (1993) 109–117.
[127] E.J. Bylaska, M. Holst, J.H. Weare, J. Chem. Theory Comput. 5 (2009) 937–948.
[128] R. Cimrman, M. Novák, R. Kolman, M. Tuma, J. Vackár ArXiv:1512.07156v1 [physics.comp-ph].
[129] J. Vackár, O. Certík, R. Cimrman, M. Novák, O. Sipr, J. Plesek, Finite element method in density functional theory electronic structure calculations, in: P. Hoggan, E. Brändas, J. Maruani, P. Piecuch, G. Delgado-Barrio (Eds.), Advances in the Theory of Quantum Systems in Chemistry and Physics, Progress in Theoretical Chemistry and Physics, Vol. 22 Springer, Netherlands, 2012, pp. 199–217.
[130] O. Kullie, H. Zhang, J. Kolb, D. Kolb, J. Chem. Phys. 125 (2006) 244303.
[131] O. Kullie, D. Kolb, Eur. Phys. J. D 17 (2001) 167–173.
[132] J.E. Pask, P.A. Sterne, Finite elements in ab initio electronic-structure calulations, in: S. Yip (Ed.), Handbook of Materials Modeling, 271 Springer, 2005, pp. 423–437 Ch. 1.19.
[133] J.E. Pask, P.A. Sterne, Modelling Simul. Mater. Sci. Eng. 13 (2005) R71–R96.
[134] J.E. Pask, B.M. Klein, P.A. Sterne, C.Y. Fong, Comp. Phys. Comm. 135 (2001) 1–34.
[135] V. Gavini, J. Knap, K. Bhattacharya, M. Ortiz, J. Mech. Phys. Solids 55 (2007) 669–696.